Single-point kinetic energy density functionals: A pointwise kinetic energy density analysis and numerical convergence investigation

Junchao Xia and Emily A. Carter

Phys. Rev. B **91**, 045124 — Published 20 January 2015

DOI: 10.1103/PhysRevB.91.045124

Single-point Kinetic Energy Density Functionals: A Pointwise Kinetic Energy Density Analysis and Numerical Convergence Investigation

Junchao Xia[1] and Emily A. Carter[1, 2,*]

[1]*Department of Mechanical and Aerospace Engineering,* [2]*Program in Applied and Computational Mathematics, and Andlinger Center for Energy and the Environment, Princeton University, Princeton, NJ 08544-5263*

Abstract

We present a comprehensive study of single-point kinetic energy density functionals (KEDFs) to be used in orbital-free density functional theory (DFT) calculations. We first propose a new form of KEDFs based on a pointwise Kohn-Sham (KS) kinetic energy density (KED) and electron localization function (ELF) analysis. We find that the ELF and modified enhancement factor have a very strong and transferable correlation with the reduced density in various bulk metals. The non-self-consistent kinetic energy errors predicted by these new KEDF models are decreased greatly compared to previously-reported generalized gradient approximation (GGA) KEDFs. Second, we perform self-consistent calculations with various single-point KEDFs and investigate their numerical convergence behavior. We find striking numerical instabilities for previous GGA KEDFs; most of the GGA KEDFs fail to converge and show unphysical densities during the optimization. In contrast, our new KEDFs demonstrate stable convergence, and their self-consistent results of various bulk

properties agree reasonably well with KSDFT. A further detailed KED analysis reveals an interesting bifurcation phenomenon in defective metals and alloys, which may shed light on directions for future KEDF development.

I. Introduction

An excellent balance between accuracy and efficiency has made Kohn-Sham (KS) density functional theory (DFT)[1] the most powerful and commonly used first principles quantum mechanical method in science and engineering today. KSDFT introduces one-electron wavefunctions to precisely calculate the non-interacting electron kinetic energy, T_s. It leaves only a small portion of the total energy, namely the exchange-correlation (XC) energy, to be approximated by density functionals. In so doing, the KSDFT formalism generally produces reliable predictions for a wide range of systems, particularly with simple local density approximations or generalized gradient approximations (GGAs) for the XC energy. However, the computational cost of standard KSDFT typically scales cubically with system size (N) due to the introduction of orbitals, which prevents its application to many large-scale ($>10^3$ atoms) systems and phenomena.

Consistent with the original Hohenberg-Kohn formalism,[2] orbital-free (OF) DFT[3] instead uses the electron density as the sole variable to calculate total energies, including T_s. Consequently, the variational degrees of freedom are reduced from $3N$ to only 3 in OFDFT, and the computational cost can be made to scale quasilinearly with N, *i.e.*, O(Nlog$N$), with a small prefactor. This extraordinary numerical efficiency is

one of its most attractive features; OFDFT simulation of over a million atoms was already feasible more than five years ago.[4] However, a tradeoff exists between efficiency and accuracy. Approximating T_s using density functionals is more difficult than approximating XC energies. The magnitude of the kinetic energy is on the same order as the total energy, which can be hundreds of times larger than XC energies. The major source of error in OFDFT therefore originates from the error in kinetic energy density functionals (KEDFs). In recent decades, numerous KEDFs have been proposed, which can be roughly categorized into two general types: two-point (nonlocal) KEDFs, featuring a double-integral form; and single-point (local/semi-local) KEDFs, which only contain a single integral.

Two-point KEDFs (*e.g.*, the Chacon-Alvarellos-Tarazona,[5-7] Wang-Teter,[8] and Wang-Govind-Carter (WGC)[9, 10] KEDFs) are generally based on Lindhard linear response theory.[11, 12] Because this theory reflects the response of a perturbed uniform electron gas, these KEDFs can achieve accuracy comparable to KSDFT for nearly-free-electron-like systems, such as main group metals. A number of studies have demonstrated their promising ability to simulate large-scale scientific problems.[13-26] Advanced two-point KEDFs have recently enabled OFDFT to describe systems with localized electrons as well, such as covalent[27-31] and transition metal systems.[32-34]

Despite the success of two-point KEDFs, researchers have continued to study single-point KEDFs for two major reasons: first, two-point KEDFs are mostly

confined to describing condensed matter, and thus we need different KEDFs for other systems, such as isolated atoms and molecules; and second, single-point KEDFs are usually numerically more efficient than two-point KEDFs, which is potentially advantageous for large-scale and molecular dynamics simulations. The history of single-point KEDFs can be traced back to the earliest KEDF approximation derived by Thomas and Fermi (TF)[35-37] as well as the well-known von Weizsäcker (vW) KEDF.[38] A large number of single-point KEDFs were subsequently proposed during the many decades of KEDF development.[39-41]

However, the development of single-point KEDFs is still rather limited. In contrast to two-point KEDF studies where self-consistent calculations are usually conducted, most single-point KEDF investigations report non-self-consistent results (i.e., KSDFT ground-state densities are input to OFDFT, and one-shot kinetic energies are calculated). Some recent studies, such as refs. 42 and 43, are notable exceptions for including some self-consistent results. Although self-consistent calculations are more demanding, they are also essential for practical applications (computation of forces, etc.). Additionally, single-point KEDF studies are usually confined to isolated systems. Development of accurate single-point KEDFs for condensed matter is still limited, although some recent studies[42-44] have investigated their performance for bulk metals (*vide infra*).

Most single-point KEDFs adopt a gradient-corrected form similar to GGA XC functionals. Enforcing certain limits, satisfying scaling requirements, and conjecturing

conjointness are widely used strategies to design the enhancement factors for these GGA KEDFs.[39-41] However, we note that most single-point KEDF studies (as well as two-point KEDF ones) focus exclusively on reproducing the total (kinetic) energy as an integrated value or derived bulk properties. Although some investigations[45, 46] have analyzed the pointwise kinetic energy density (KED or τ) and computed average KED errors, very few[47, 48] have attempted to analyze the KED distribution for the purpose of designing new KEDFs. While studying pointwise quantities is more difficult than calculating T_s as an integrated value, it can reveal interesting problems. As an example, the sole variable in the enhancement factor of many GGA KEDFs is the reduced gradient ($s(\mathbf{r}) = |\nabla\rho| / \rho^{4/3}$). However, the KSDFT KED is not a single-valued function of s (*vide infra*), which calls into question the use of enhancement factors dependent on s alone. Their integrated total energy thus may involve considerable error cancellation to achieve accuracy comparable to KSDFT.

The aim of this work is consequently twofold. First, we propose a new form of single-point KEDFs based on a pointwise quantity analysis. In addition to the most fundamental pointwise quantity KED, we also investigate other closely-related quantities, such as the electron localization function (ELF).[49, 50] The ELF also contains a key quantity (noted as G in this paper), which is defined as the difference between the KED and local vW KED normalized by the local TF KED (see Equation (8) in Sec. II). Note that this quantity is used in recently proposed meta-GGA XC functionals.[51] Since the local TF and vW KEDs can easily be computed, calculating the ELF/G using density functionals is equivalent to calculating the KED. However,

compared to the total kinetic energy or KED, *G* provides more information, such as bond types.[51] Similarly, the ELF (solely dependent on *G*) can also give more physical meaning in terms of electron localization or delocalization; its distribution is largely determined by the system type and crystal structure. We will therefore focus on studying KED/ELF/*G* distributions, aiming to find a strong and transferable correlation between these distributions and electron density variables, and construct accordingly OF KED/ELF/*G* and thus corresponding KEDFs. We will show that our new KEDFs can produce reasonable non-self-consistent as well as self-consistent results for various materials, indicating great improvement over previous single-point GGA KEDFs.

Second, we provide a systematic test of single-point KEDFs' performance for condensed matter within pseudopotential schemes (only containing valence electrons), which has been missing in literature until now. We test various previous GGA KEDFs and our new single-point KEDFs by comparing both non-self-consistent kinetic energies and self-consistent bulk properties against KSDFT benchmarks. As mentioned above, most GGA KEDF studies have only reported non-self-consistent results; the difficulty in performing self-consistent GGA KEDF calculations is related to singularities near nuclear positions in all-electron calculations[40, 44] (to be fair, some successful self-consistent calculations for several GGA KEDFs with pseudopotentials have been reported).[44] However, we will show that most GGA KEDFs cannot obtain stable and physically reasonable self-consistent results, even within the pseuodopotential approximation.

The paper is organized as follows. We present our new single-point KEDF formalism in Sec. II and provide computational details in Sec. III. We then test our models in Sec. IV against representative single-point and two-point KEDFs on metallic systems. Non-self-consistent results, instability issues with GGA KEDFs, self-consistent results, a detailed KED distribution analysis, and possible future improvements are discussed. Finally, conclusions are given in Sec. V.

II. Theory and formalism

GGA KEDFs have the general form:

$$T_s[\rho] = \int \tau_{TF} F(s) d\mathbf{r} \text{ , (1)}$$

where τ_{TF} is the TF KED, s is the reduced gradient, and $F(s)$ is the enhancement factor. Here, we take an alternative point of view to propose a slightly different KEDF form. To begin, recall that the total kinetic energy is by definition an integral of the KED:

$$T_s[\rho] = \int \tau(\mathbf{r})[\rho] d\mathbf{r} \text{ , (2)}$$

where the local KED (τ) is in general a functional of the total electron density, such as the orbital-based KED within the KS method. We can further write the KED as

$$\tau(\mathbf{r}) = \tau_{vW}(\mathbf{r}) + \tau_{TF}(\mathbf{r}) G[\rho] \text{ , (3)}$$

where $\tau_{TF} = C_{TF}\rho^{5/3}$, $C_{TF} = 3/10(3\pi^2)^{2/3}$, and $\tau_{vW} = \frac{1}{8}\frac{|\nabla\rho(\mathbf{r})|^2}{\rho(\mathbf{r})}$. As a result, we write the general form of KEDF as

$$T_s[\rho] = T_{\mathrm{vW}} + \int \tau_{TF} G[\rho] d\mathbf{r} \ . \ (4)$$

This form is very similar to the GGA form; we simply subtract the vW term out and note that $F = F_{\mathrm{vW}} + G$, where $F_{\mathrm{vW}} = \frac{s^2}{8C_{\mathrm{TF}}}$ is the enhancement factor of the vW KEDF. There are some subtleties and advantages of this new form. First, up to this point, Equation (4) is exact: *G* should be a functional of the electron density instead of a function of *s*. Although *s* is a very important quantity, it does not provide all the information necessary to build an accurate KEDF. In KSDFT, the KED or *G* is calculated with orbitals that can be considered as a functional of the electron density. Furthermore, one can think of two-point functionals as having a functional form of *G*. For example,

$$G^{\alpha}_{\mathrm{WGC}}[\rho] = 1 + \int \frac{\rho^{\alpha}(\mathbf{r})}{\tau_{\mathrm{TF}}(\mathbf{r})} \omega \rho^{\beta}(\mathbf{r}') d\mathbf{r}' \ , \ (5)$$

or

$$G^{\beta}_{\mathrm{WGC}}[\rho] = 1 + \int \frac{\rho^{\beta}(\mathbf{r})}{\tau_{\mathrm{TF}}(\mathbf{r})} \omega \rho^{\alpha}(\mathbf{r}') d\mathbf{r}' \ , \ (6)$$

or normalized linear combinations of these two (KS KED or *G* also has multiple definitions, as discussed below), where ω is the kernel function and α and β are constants. Second, the form of Equation (4) is closely related to the idea of the Pauli term (given by the total kinetic energy minus the vW term), as discussed in several previous papers.[40, 52] Since T_{vW} is separated out, the positive-definite property of the remaining term (namely the Pauli term), as well as its pointwise Pauli potential,[40, 52]

can be relatively easily checked and guaranteed when constructing G. Finally and most importantly, we note that G by definition is naturally connected to the ELF as

$$G[\rho] = \frac{\tau - \tau_{vW}}{\tau_{TF}}, \quad (7)$$

$$ELF(\mathbf{r}) = \frac{1}{1 + \left(\frac{\tau - \tau_{vW}}{\tau_{TF}} \right)^2} = \frac{1}{1 + G^2}, \quad (8)$$

and thus,

$$G = \sqrt{\frac{1}{ELF} - 1}. \quad (9)$$

By substituting Equation (9) into Equation (4), we have

$$T_s[\rho] = T_{\mathrm{vW}} + \int \tau_{TF} \sqrt{\frac{1}{ELF[\rho]} - 1} d\mathbf{r}, \quad (10)$$

which can connect some studies of OF-ELF[53] to KEDF development. However, no approximation has been made up to this point, and the fundamental problem still exists: can we approximate G using solely the electron density?

We next employ a different approach from many previously proposed KEDFs to determine G. Instead of designing our KEDF to match integrated quantities, such as KSDFT total energies or bulk properties, we construct KEDFs based on pointwise quantities (*e.g.*, the KED). In the following, we investigate pointwise local KED/ELF/G distributions from KSDFT, and their dependence on different density variables (*e.g.*, the electron density, s, and the reduced Laplacian). Clearly, if we can

obtain accurate KED values at every point in space, then the total kinetic energy (an integrated quantity) will be inherently accurate.

We employ KSDFT data as our benchmark because it gives the exact non-interacting KED values needed. The G value can be easily computed for each point in space using Equation (7). However, an issue may arise from the ambiguous definition of the KSDFT τ. Two definitions, $\tau_{\mathrm{KSDFT}} = \sum_k f_k \left|\nabla \varphi_k\right|^2 / 2$ and $\tau_{\mathrm{KSDFT}} = -\frac{1}{2}\sum_k f_k \varphi_k \nabla^2 \varphi_k = \sum_k f_k \left|\nabla \varphi_k\right|^2 / 2 - \frac{1}{4}\nabla^2 \rho$,[54] are commonly used in the literature, where k refers to the index of the KS orbitals and f_k is the occupation number. Moreover, one can prove that any divergence of periodic functions (*e.g.*, $\nabla \cdot \nabla \rho$) can be added and has no contribution to the total kinetic energy. For example,

$$\tau = \sum_k \left|\nabla \varphi_k\right|^2 / 2 + x \cdot \nabla^2 \rho \text{ , (11)}$$

has also been used,[45, 46] where x can be an arbitrary number. We will however mainly adopt $\tau = \sum_k f_k \left|\nabla \varphi_k\right|^2 / 2$ in this work (all results shown use this definition unless stated otherwise) due to its positive-definite property. Moreover, this definition of τ enforces the pointwise version of the vW lower bound criterion for the kinetic energy, and is consistent with the ELF definition.

We next aim to investigate the relation between KSDFT KED/ELF/G and various density variables. We first examine the dependence of the ELF on the reduced density d (ρ/ρ_0, where ρ_0 is the average density in the unit cell) in several bulk metals. Figure

1 shows the ELF vs. d along the bond axis in face-centered cubic (fcc) Al, hexagonal-close-packed (hcp) Mg, and body-centered-cubic (bcc) Li at their equilibrium volumes. Remarkably, we see a nearly single-valued function relating the ELF and d. Furthermore, when $d=\rho/\rho_0=1$, the ELF is approximately 0.5, which is the correct limit for the uniform electron gas. The use of the reduced density in KEDFs is uncommon, especially in single-point KEDFs. However, the positive correlation between the ELF and d does make physical sense. Qualitatively, the electron density will be large when electrons are localized, and, thus, larger d will correspond to higher ELF values. For sure, this correlation is not exact; a very simple counterexample is any single-orbital system (*e.g.*, Li_2 in a pseudopotential formalism) where the ELF is constantly 1 but the reduced density cannot be flat (for isolated systems, ρ_0 is actually ill-defined but the dimensionless quantity ρ/ρ_{max} may be used instead). However, this approximate correlation between the ELF and d generally works well for condensed matter. Our earlier work[29] also supports the use of d to determine the level of electron localization in covalent systems (see Figure 1 in ref. 29).

According to Equation (9), the ELF has a one-to-one mapping to G. Since the ELF features a nice correlation with d, we expect d to be a good descriptor for G as well. Moreover, predicting G directly would be more convenient and straightforward for use in a KEDF. Figure 2 therefore shows G vs. d from all spatial points (on a numerical grid) in the unit cell of bcc Li (the curves are very similar for other phases). Figure 3 then displays G vs. d data along the bond axis in different phases of Al, Mg,

and Li at equilibrium volumes and under deformations. Several appealing properties emerge: (1) The data from all systems collapse onto the same curve, indicating good transferability on a pointwise level for the KED within these metallic phases. (2) The data form a well-defined single-valued function of d. This is important because approximating G as a function of any independent variable would make sense only if G is a well-defined, single-valued function of the independent variable. We will later see that G vs. s does not share this behavior. (3) G is approximately 1 ($\mathrm{ELF} \approx 0.5$) when d=1. For the uniform electron gas ($\rho \equiv \rho_0$, $d \equiv 1$, and $\tau_{\mathrm{vW}} \equiv 0$), $G \equiv 1$ then leads to the pure TF KEDF, which is the correct limit we hope to preserve.

Based on the strong and transferable correlation found between G and d, we propose several simple KEDF models by approximating G as a function of d. Note that although G depends on only d, the corresponding traditional enhancement factor $F = F_{\mathrm{vW}} + G$ is a function of both d and s. We can either directly fit G vs. d (Figure 3) to obtain $G(d)$, or fit ELF vs. d (Figure 1) and use Equation (10) to calculate T_s. For our first KEDF model, we conduct a linear fitting for ln(G) vs. ln(d) (Figure 4) using data along the bond axis in fcc Al, bcc Li, and hcp Mg at their respective equilibrium volumes. This leads to

$$G(d) = a \cdot d^b \quad , (12)$$

with a = 0.9892 and b = -1.2994. We refer to this model as vWGTF1 (τ_{vW} plus G times τ_{TF}) below. For our second KEDF model, we propose the following analytical form of ELF(d),

$$ELF(d) = \left(1 + \tanh(p \cdot d^q - p)\right)/2, \quad (13)$$

and numerically determine the parameters using a least squares fitting. The final parameters are p=5.7001 and q=0.2563. Equation (13) guarantees the ELF bound within 1 when d approaches infinity, and ELF(1) is 0.5 by construction. The ELF raw data and fitted analytical function are plotted in Figure 5. This KEDF is referred to as vWGTF2.

The vWGTF1 and vWGTF2 KEDFs are fundamentally similar; the former fits G directly while the latter fits the ELF first, and then uses the exact relation between G and ELF, *i.e.*, Equation (9). Fitting G is more straightforward and naturally forces the ELF to satisfy the bound between 0 and 1. Furthermore, the positive-definite property of the Pauli energy and the pointwise Pauli potential can be more easily guaranteed when directly fitting G. Simple calculations confirm that the vWGTF1 model indeed guarantees the positive-definite property for both the Pauli energy and its potential with any electron density. The vWGTF2 KEDF guarantees positive definiteness for the Pauli energy; however, the Pauli potential can be negative with large d values (d~2). Nevertheless, we still propose the vWGTF2 model because it highlights the connection between the ELF and G. We think the ELF contains deeper physical meaning than G, and it is well-established and studied in literature. Fitting the ELF thus connects KEDF development to those ELF studies.

We have thus far approximated G as a function of d. Strictly speaking, the resulting vWGTF KEDFs are not single-point functionals, as ρ_0 in d depends

non-locally on the whole system. This may lead to size-consistency issues for non-homogenous systems, such as surfaces and interfaces. Generally, when deploying KEDFs (such as the WGC) that involve ρ_0, we take ρ_0 to be the average of the density but only over the space where densities are larger than a threshold, such as the minimum density in the corresponding bulk system (e.g., bulk fcc Al for fcc Al surface calculations). This method largely eliminates a potential size-consistency problem for surfaces modelled in a periodic cell (energies should not depend on the thickness of the vacuum layer). However, this approach may not always work for the heterogeneous interface case. For this reason, it could be more desirable to use purely local variables. We thus next consider using s (purely local) as the independent variable instead. Unfortunately, we fail to observe a well-defined correspondence between G and s, namely a single-valued function $G(s)$. Figure 6 shows G vs. s in fcc Al calculated with KSDFT. Multiple branches exist with various possible x values in Equation (11), *i.e.*, we have multiple corresponding G values for each s. Consequently, it is not sensible to predict G using only s. Since G and F are basically equivalent under the current approximation (the difference being F_{vW}), this multivalued character calls into question the validity of the GGA's $F(s)$. However, this does not mean that s cannot be included in G or F. A combination with other density variables, or multi-variate G functions/functionals including s, might very possibly improve the model.

The density Laplacian $\nabla^2\rho$ is another informative and important quantity when constructing KEDFs, as it helps to determine bond types[55] and is a strong indicator of

electron accumulation or depletion. We observe a much better relationship between G and the reduced Laplacian ($l = \nabla^2\rho/\rho^{5/3}$) than with s, though it is not as good as G vs. d. However, inclusion of l complicates the kinetic potential and makes self-consistent optimizations unstable (see discussion in Sec. IV). For simplicity, we will consider the G function using only d. We will however highlight the importance of l in Sec. IV when discussing cubic diamond (CD) Si.

III. Computational details

We study Al, Mg, and Li bulk phases, as well as $\beta''-Al_3Mg$, CD Si, and the singlet state of the P_2 molecule using KSDFT and OFDFT. We carry out all KSDFT calculations with the ABINIT package[56] and OFDFT calculations with our PROFESS 3.0 code.[57-59] The Perdew-Burke-Ernzerhof (PBE) GGA XC functional[60] is employed in all calculations. Bulk-derived local pseudopotentials[28, 61, 62] are used in both KSDFT and OFDFT. A 900 eV KE cutoff is used in KSDFT calculations for the plane-wave basis to converge the total energy to within 1 meV/atom. 20×20×20 k-point grids are used for all crystals. **k**-point meshes were generated with the Monkhorst-Pack method.[63] 1 **k**-point is used for P_2. Fermi-Dirac smearing is used for all Al, Mg, Li, and Al_3Mg calculations, with a smearing width equal to 0.1 eV. No smearing is used for CD Si or P_2 calculations.

In self-consistent OFDFT calculations, the ground-state energy is obtained by optimizing the electron density (see details in ref. 57). The optimizations are all derivative-based, and the kinetic potential can be calculated via functional derivative

calculations. However, we find some analytically equivalent expressions can lead to different numerical behavior; we discuss this issue in Sec. IV B. In our implementations, we apply the general analytical formula for all GGA KEDF potentials:

$$\frac{\delta T_s}{\delta \rho} = \frac{\partial \tau_{TF}}{\partial \rho} \cdot F(s) + \tau_{TF} \cdot \frac{\partial F}{\partial s} \cdot \frac{\partial s}{\partial \rho} - \nabla \cdot \left(\frac{\partial F}{\partial s} \cdot \frac{\partial s}{\partial (\nabla \rho)} \right), \quad (14)$$

where $\frac{\partial \tau_{TF}}{\partial \rho} = \frac{5}{3} C_{TF} \rho^{2/3}$, $\frac{\partial s}{\partial \rho} = -\frac{4}{3} \frac{s}{\rho}$, $\frac{\partial s}{\partial (\nabla \rho)} = \frac{\nabla \rho}{|\nabla \rho| \rho^{4/3}} = \frac{\nabla \rho}{s \cdot \rho^{8/3}}$, and each GGA KEDF has its corresponding $\frac{\partial F}{\partial s}$. In plane-wave-based PROFESS, numerical gradient and divergence operations are all realized via the fast Fourier transform (FFT). Specifically,

$$\nabla f(\mathbf{r}) = \hat{F}^{-1}\{i\mathbf{g} \cdot \tilde{f}\}, \quad (15)$$

and

$$\nabla \cdot \mathbf{f}(\mathbf{r}) = \hat{F}^{-1}\{ig_x \tilde{f}_x + ig_y \tilde{f}_y + ig_z \tilde{f}_z\}, \quad (16)$$

where $\tilde{f}$ is the Fourier transform of any integrable function f, $\mathbf{g}$ is the reciprocal (momentum space) vector, and $\hat{F}^{-1}$ is the inverse Fourier transform operator.

In all OFDFT calculations, the kinetic energy cutoff is set at 1600 eV. However, many GGA KEDFs are numerically unstable; they cannot be converged even with very high kinetic energy cutoffs, as demonstrated by both their total energies and unphysical densities (see Sec. IV B). The 1600 eV kinetic energy cutoff converges the total energy to within 1 meV/atom for the GGA functionals that are numerically

stable, the WGC99 (hereafter just referred to as WGC) KEDF,[10] and the new vWGTF KEDF models proposed in this work.

We test TF, vW, TFλvW with λ equal to 1/5,[64-68] 1/9,[69] and 1,[68] Lee-Lee-Parr (LLP),[70] DePristo-Kress (DK),[71] DK87,[72] Ou-Yang-Levy 1 (OL1),[73] OL2,[73] Perdew-Wang 86 (PW86),[74, 75] PW91,[76] Lembarki and Chermette (LC94),[77] Tran-Wesolowski (TW02),[78] PBE2,[79] E00,[80] P92,[81] Becke 86A (B86A),[82] Becke 86B (B86B),[83] and Thakkar (Thak)[84] GGA functionals, with the parameters proposed in their original papers. Their corresponding G can be calculated simply as $G=F-F_{\mathrm{vW}}$.

The two-point WGC KEDF contains, in addition to TF and vW terms, a double-integral nonlocal term:

$$E_{\mathrm{NL}}^{\mathrm{WGC}}=\int\int\rho^{\alpha}(\mathbf{r})\omega\left(\xi(\mathbf{r},\mathbf{r}')|\mathbf{r}-\mathbf{r}'|\right)\rho^{\beta}(\mathbf{r}')d\mathbf{r}d\mathbf{r}', \quad (17)$$

where the kernel ω is determined by recovering the exact Lindhard linear response for the perturbed uniform electron gas, and ξ is a two-point Fermi wavevector that is thus double-density-dependent: $\xi(\mathbf{r},\mathbf{r}')=\left(\frac{k_F^{\gamma}(\mathbf{r})+k_F^{\gamma}(\mathbf{r}')}{2}\right)^{1/\gamma}$ with $k_F^{\gamma}(\mathbf{r})=\left(3\pi^2\rho(\mathbf{r})\right)^{1/3}$. Furthermore, to remain quasi-linear scaling via using FFTs, the density-dependent kernel is Taylor-expanded around the center ρ^*. In this work, the optimal parameters $\alpha=(5-\sqrt{5})/6$, $\beta=5/3-\alpha$, $\rho^*=\rho_0$, and γ=2.7 are used in all WGC KEDF calculations,[9, 10] except for CD Si for which γ=3.6 is used in order to guarantee numerical convergence with large density fluctuations present.[85] Parameters of vWGTF1 and vWGTF2 KEDFs are given in Sec. II above.

Non-self-consistent kinetic energy errors are simply calculated using converged KSDFT densities output from ABINIT. For self-consistent results, we calculate equilibrium volumes (V_0) and bulk moduli (B) for fcc, hcp, bcc, and simple cubic (sc) Al, Mg, Li, and $\beta''-Al_3Mg$. The equilibrium structures are obtained by relaxing ion positions and cell lattice vectors with default force and stress thresholds in ABINIT. In OFDFT calculations, the equilibrium volume is found by expanding and compressing unit cells and finding the total energy minimum. The *c*/*a* ratio in hcp structure is obtained by manually scanning the ratio; there are no degrees of freedom in atom positions or cell lattice vectors in other structures. The bulk modulus is calculated with Murnaghan's equation[86] to fit total energy vs. volume data within a ±2% range around the equilibrium volume. In addition, the phase energy differences are calculated for various Al, Mg, and Li phases as the total energy differences between phases at their equilibrium volumes.

We also calculate vacancy formation energies in fcc Al, hcp Mg, and bcc Li. A 2×2×2 supercell (31 atoms), 3×3×2 supercell (35 atoms), and 2×2×2 supercell (15 atoms) with one atom removed at the origin are used for fcc Al, hcp Mg, and bcc Li vacancy calculations, respectively. The structures are not relaxed in either KSDFT or OFDFT calculations, since we only aim to compare KSDFT and OFDFT under identical situations; in our experience, relaxation will not lead to large differences for these simple metals. The vacancy formation energies are then calculated using Gillan's expression:[87]

$$E_{vf} = E\left(N-1,1,\frac{N-1}{N}\Omega\right) - \frac{N-1}{N}E(N,0,\Omega)\,, \quad (18)$$

where $E(N,m,\Omega)$ is the total energy for a cell with volume Ω, N atoms, and m defects.

The primitive unit cell of $\beta''-\mathrm{Al_3Mg}$ is employed to model the bulk alloy. The alloy formation energy per atom is then calculated as

$$\Delta E_{\mathrm{f}} = (E_{\mathrm{Al_3Mg}} - 3E_{\mathrm{Al}} - E_{\mathrm{Mg}})/4\,, \quad (19)$$

where $E_{\mathrm{Al_3Mg}}$ is the total energy per primitive cell of $\beta''-\mathrm{Al_3Mg}$, while E_{Mg} and E_{Al} are total energies per atom in hcp Mg and fcc Al at their respective equilibrium volumes.

Finally, only the nonmagnetic (M_S=0) state is examined in P_2 KSDFT calculations. Two atoms are set up in the center of a $20\times10\times10$ Å^3 cell, aligned along the longest direction. The equilibrium bond length (r_e) is obtained by varying the bond length in a wide range and finding the total energy minimum. All data shown in Sec. IV are computed at r_e.

IV. Results and Discussion

A. Non-self-consistent results

Here we discuss non-self-consistent OFDFT results, *i.e.*, using the KSDFT density directly in OFDFT calculations to calculate the kinetic energy without further density optimization. This is considered the standard test in most of the earlier GGA KEDF

studies. Although the focus of this work is on single-point KEDFs, we include two-point WGC KEDF results for comparison because it is thus far the most successful KEDF for the systems studied here.

In Table I, kinetic energy errors (in %) compared to KSDFT benchmarks, computed with various KEDFs, are given for different bulk main group metal phases. First, using the vW KEDF alone produces extremely inaccurate results. Since these particular metals have density distributions close to the uniform-electron-gas limit, the TF performs much better than the vW but the former still significantly underestimates the kinetic energy. Most of the GGA KEDFs produce rather poor results, with mean absolute errors (MAEs) around 3-6%. The parameters in those KEDFs were fit to data from isolated atoms or molecules, so their unsatisfactory performance in these bulk metals is somewhat expected. A large group of KEDFs behave very similarly in their underestimation of the kinetic energy, *e.g.*, the TF1/9vW, PW91, TW02, *etc*. Those functionals feature similar asymptotic behavior around s=0 (*e.g.*, see Table I in ref. 79); they consequently behave quite similarly with the metals considered here, where s is relatively small.

On the other hand, the PBE2 and TFvW are different from other GGA KEDFs, as they both overestimate the kinetic energy compared to KSDFT benchmarks. This can also be attributed to their similar small s behavior.[79] Their vW parts have much larger coefficients than other GGA KEDFs when expanding around s=0, which tends to over-correct the kinetic energy. Moreover, among all the GGA KEDFs, TFvW is the

best based on these kinetic energy errors. Theoretically, this form does not have strong physical justification as a simple combination of two best-known functionals. However, its accuracy for these systems is not surprising, since the TF and vW KEDFs are the leading terms in the WGC KEDF, which is known to be accurate for such systems (as also shown in Table I), and also the nonlocal term is usually not large. In contrast to GGA KEDFs, our new vWGTF KEDFs exhibit considerably improved accuracy for all test cases. The MAEs of vWGTF KEDFs are much smaller than 1% and just a bit larger than the WGC KEDF, which is the best for all metals, as expected. Given that the parameters in the vWGTF KEDFs are fit using only ground-state phases and data points strictly along the bond axis, the results here show quite reasonable transferability, at least in the metallic phases considered.

We also test vacancy structures for fcc Al, hcp Mg, and bcc Li and for one alloy Al_3Mg (Table II). The mean absolute errors incurred when describing vacancies decrease slightly for most of the GGA KEDFs, while the WGC KEDF error increases modestly, which nevertheless is still very accurate (with errors much less than 1%). The vWGTF models still exhibit errors within 1%, much smaller than all the GGA KEDFs (mostly above 4%).

B. Numerical convergence in self-consistent calculations

Self-consistently solving the Euler equation is required to use OFDFT in real applications,[57] which is more demanding both physically and numerically than non-self-consistent calculations. Only simultaneously guaranteeing correct kinetic

energies and potentials can lead to accurate energetics, as well as correct ground-state densities. Many GGA KEDFs have unphysical kinetic potentials,[40] and consequently suffer from either numerical instabilities or produce unphysical results after self-consistent density optimization. In this section, we provide a systematic test of convergence stability in self-consistent calculations for different KEDFs.

We first find significant numerical difficulties when solving self-consistently for almost all GGA KEDFs, except for TFλvW, E00, and P92. The difficulties of self-consistent OFDFT calculations with GGA KEDFs for all-electron calculations were discussed in ref. 44. The singular and unphysical behavior of the kinetic potential around the nucleus makes self-consistent calculations unstable and hard to solve.[40, 44] The pseudopotential approximation should remove the singularity issue, and one may expect better stability. In fact, in ref. 44, self-consistent results were reported for bulk Li and Al phases calculated with a modified version of PROFESS. However, we find that the pseudopotential approximation does not ensure convergence with GGA KEDFs; most of the GGA KEDFs continue to be extremely numerically unstable, although the simple metallic systems investigated here feature rather small density fluctuations. For the PW91, TW02, PBE2, LC94, PW86, B86A, and B86B KEDFs, we can obtain energy minima after density optimizations but their total energies cannot be converged with respect to the plane-wave basis kinetic energy cutoff (they change greatly as the energy cutoff increases). Consequently, the resulting energy vs. volume curves are not smooth at all. For example, Figure 7 shows fcc Al energy vs. volume curves calculated with the PBE2 KEDF with different

kinetic energy cutoffs. When the kinetic energy cutoff is 500 eV, the curve looks smooth, the same as shown in ref. 44. However, when the kinetic energy cutoff increases, we can no longer obtain meaningful energy vs. volume curves, and the energies are clearly not converged with respect to the kinetic energy cutoff (even up to 20,000 eV, a huge kinetic energy cutoff, as we tested but not shown here). Other GGA KEDFs, including the OL1, OL2, LLP, Thak, DK, and DK87, feature even worse behavior during self-consistent optimizations; optimizers usually cannot find any energy minima, as their energies diverge to unphysical, extremely negative values during the optimization.

Analyzing electron densities during the optimization illuminates the instability issue further. In Figure 8, the density distributions of fcc Al after self-consistent optimization are plotted for many different KEDFs. For those GGA KEDFs that can achieve robust self-consistent results, such as the TFvW, TF1/5vW, and E00 KEDFs, their final densities are smooth and physical, although some of them are not close to the KSDFT benchmark. However, for the other GGA KEDFs, we find that their densities are frequently trapped in unphysical states, which may be the origin of the convergence problem. Specifically, for the likes of PBE2 and TW02, their densities around nuclei become unphysically small. With increasing kinetic energy cutoffs, the local density can decrease to less than 10^{-100} $bohr^{-3}$, which should not appear in fcc Al. The densities then abruptly increase to large values around 2 bohr from the nuclei (around 0.2 in normalized units in Figure 8). We also observe sharp density oscillations for the PW91 and PBE2 KEDFs. Those step-function-like extremely

rapidly changing densities cannot be described accurately using a plane wave basis, so convergence and stability issues during self-consistent calculations should be anticipated.

We find that a similar problem exists not only for those GGA KEDFs with complicated *F* but even for the simple vW KEDF. Analytically equivalent expressions may exhibit different numerical behavior. For example, as mentioned earlier two commonly used definitions exist for the vW KEDF: $E_{\mathrm{vW}} = \int \frac{|\nabla\rho|^2}{8\rho} d\mathbf{r}$ and $E_{\mathrm{vW}} = -\frac{1}{2}\int \sqrt{\rho}\nabla^2\sqrt{\rho} d\mathbf{r}$. Analytically, these two definitions are exactly the same, since they simply differ by a term proportional to the Laplacian of the density (they have identical kinetic potentials). However, they are not identical numerically. In most calculations where densities stay physically reasonable, these two definitions indeed behave similarly. When using the first definition, however, densities occasionally are unphysical (extremely small density regions or sharp changes) and energies can no longer converge. In contrast, the latter implementation generally guarantees a physical solution in our tests. Further testing shows that even when unphysical densities are provided for the initial guess, the second expression can recover from divergences and converge to a physically reasonable answer. Moreover, with unphysical densities, two theoretically identical total energies are vastly different from each other. These observations imply that at least one of the definitions is not calculating the quantity correctly (presumably the first one). They also indicate that we may need to use different analytically equivalent expressions for the other GGA

kinetic potentials. Unfortunately, it is hard to systematically find equivalent and more numerically stable expressions than Equation (14) for various GGA KEDFs, especially for those with complicated enhancement factors. We have tried several alternatives for the PBE2 and TW02, but all lead to similar convergence problems.

With these unphysical densities, we believe that the numerical evaluation is not calculating the real functionals, just as we confirmed in the vW case. We therefore tested some other methods, such as adding penalty terms and providing exact KSDFT or WGC KEDF self-consistent densities as initial guesses, aiming to prevent densities from going into unphysical states during the optimization. However, none of these attempts worked and hence it is still unknown how the "correct" self-consistent results can be obtained for these GGA KEDFs. Thus, another obstacle to developing KEDFs arises, in that one has to consider if the KEDF is numerically stable in self-consistent calculations. Indeed, this numerical instability exhibited by many of the GGA KEDFs may be the reason why so few self-consistent calculations were reported in previous work.

By contrast, the vWGTF KEDFs can be converged self-consistently. The difference in numerical stability should not be due to using G instead of F, since fundamentally any KEDF using F can be rearranged to the form with G. Instead, we think the convergence issue of many GGA KEDFs is related to use of the reduced gradient or Laplacian. As mentioned above, even the vW KEDF can show numerical instability when using a different implementation. The E00 and P92

KEDFs do converge, but usually require much more iterations. Furthermore, when we include the Laplacian in the vWGTF models, the numerical convergence also becomes unstable.

C. Self-consistent results

We compare material properties from self-consistent calculations in this section. In Tables III-V, equilibrium volumes, bulk moduli, and phase ordering energies for different bulk phases of Al, Mg, and Li are listed, respectively. Only those convergeable GGA KEDF (TFλvW, E00, and P92) results are included due to the issue discussed above. Among said GGA KEDFs, the TFvW model again appears to be the best, though large errors still exist compared to KSDFT. The E00 and P92 share the same conjointness form, which may be the reason why both KEDFs can converge. The P92 has the second order gradient expansion approximation asymptotic behavior (TF plus 1/9vW) when s is around 0, and it consequently leads to very similar results as TF1/9vW. Overall, these GGA KEDFs give rather unsatisfactory results, greatly overestimating equilibrium volumes, underestimating bulk moduli, and producing inaccurate energy differences.

On the other hand, our new vWGTF KEDFs show very good agreement with KSDFT benchmarks for both electron densities (Figure 8) and energetics. The vWGTF densities almost overlap with the KSDFT benchmark. Furthermore, almost all equilibrium volumes have less than 3% error, corresponding to <1% errors for lattice constants. In addition, their bulk modulus predictions are very accurate for Mg

and Li phases, while the vWGTF1 KEDF overestimates (by ~10 GPa) the bulk moduli of most Al phases. The phase orderings are correct overall, and energy differences are fairly close to KSDFT benchmarks, except for the Al hcp structures where the energy difference from fcc is within just tens of meV/atom. Considering the relative accuracy of OFDFT and the simple model used here, all the bulk properties of the vWGTF models agree quite well with KSDFT results, and are the best among all single-point KEDFs. The results further demonstrate the transferability of the vWGTF KEDFs from the perspective of total energies and bulk properties, in addition to the pointwise KED perspective (Figure 3).

The WGC KEDF is not surprisingly the best among all KEDFs, producing almost identical results as KSDFT. However, the accuracy shown by vWGTF KEDFs is still impressive, and their computation time is 3-4 times faster than WGC KEDF calculations. When performing large-scale molecular dynamics simulations that may take weeks or months, this efficiency increase is considerable. To put these comparisons in context, the simple TFλvW KEDF is only ~5 times faster than the WGC KEDF; the bare TF can be ~15 times faster (for each energy and potential calculation), but it is highly inaccurate and requires many more iterations to converge due to its unphysical description of the system. Other convergable single-point KEDFs (like E00 and P92) usually take much longer than the WGC KEDF due to large number of iterations needed. We thus consider the efficiency of the vWGTF KEDFs to be fairly reasonable, being only ~1.5 times slower than the TFλvW KEDFs.

Thus, switching from TFλvW to vWGTF KEDFs can offer much better accuracy while sacrificing little in efficiency.

To further test single-point KEDFs, we consider less uniform cases, such as vacancies in fcc Al, hcp Mg, and bcc Li (Table VI), as well as a simple alloy Al_3Mg (Table VII). For these systems, we only show KSDFT, WGC, and vWGTF results, since all other KEDFs either produce very poor results or fail to converge. The WGC KEDF again predicts very accurate results compared to KSDFT benchmarks. The vWGTF models still give fairly reasonable but larger errors for Al_3Mg bulk properties and the bcc Li vacancy formation energy, respectively. However, the vWGTF KEDFs fail to reasonably describe vacancies in fcc Al and hcp Mg, giving rise to negative vacancy formation energies. Furthermore, they greatly overestimate the magnitude of the Al_3Mg alloy formation energy, although they give the correct negative sign. The failure of vWGTF models on these defective and alloy materials show their insufficient transferability beyond perfect, single-element bulk metals. In the next section, we further analyze the reason of their failure from a pointwise KED point of view.

D. Pointwise analysis

All results shown above are based on total (kinetic) energies. As mentioned in previous sections, pointwise quantities, such as the KED, ELF, or *G* provide more rigorous and illuminating information than total energies. In this section, we will

compare different KEDFs on a pointwise level, with a particular focus on G vs. d distributions.

We have already shown that the WGC KEDF can accurately describe various metals on an integrated level (Sec. IV A and C, respectively). We next want to investigate how it performs for more demanding pointwise quantities. However, as mentioned in Sec. II, the definition of G_{WGC} is not unique, since it is a two-point KEDF. Two natural ways to define G_{WGC} are Equation (5) and Equation (6), depending on which local coordinates are chosen, while the linear combination of these two definitions, $G_{WGC} = c \cdot G^{\beta}_{\mathrm{WGC}}[\rho] + (1-c) \cdot G^{\alpha}_{\mathrm{WGC}}[\rho])$, is also a valid definition. In the following, we employ a simple average definition with c=1/2, *i.e.*, $G_{WGC} = (G^{\beta}_{\mathrm{WGC}}[\rho] + G^{\alpha}_{\mathrm{WGC}}[\rho])/2$. We find that while each of these definitions produces somewhat different G values, the general characteristics of the corresponding G vs. d distributions are similar. As a result, we emphasize qualitative behavior rather than absolute values in the following G vs. d analysis.

In Figure 9, we plot G vs. d data for fcc Al calculated by KSDFT and OFDFT with the WGC, vWGTF, and some representative GGA KEDFs. The WGC curve is very close to the KSDFT data. The absolute errors are a bit larger in the small d region, but here they have smaller contributions to the total kinetic energy (τ_{TF} is small). These results may not be surprising, since the WGC KEDF is designed to describe such a metal; the results are, however, still amazing because previous results showed only accurate total energies without examining anything on a pointwise level.

Turning to single-point KEDFs, all vWGTF data are very close to those of KSDFT. The accuracy here is expected because our vWGTF models were fit to generate accurate G values, and we have confirmed their transferability already. The G distributions of other GGA KEDFs are generally very different from KSDFT, indicating that they will predict rather poor local quantities, such as the KED. Furthermore, one can expect them to demonstrate inaccurate pointwise kinetic potentials from Sec. IV B because during a self-consistent optimization, the density changes greatly starting from the KSDFT density initial guess and finally falls into an unphysical state. By contrast, both WGC and vWGTF OFDFT calculations converge in just a few iterations, with final densities very close to KSDFT (Figure 8). This also suggests the pointwise kinetic potentials of the WGC and vWGTF models are accurate.

Thus far, we have excellent agreement of the WGC and vWGTF KEDFs compared with KSDFT on an integrated and a pointwise level for bulk metals. We next inspect defective and alloyed metals for which we observed failures in the previous section for the vWGTF KEDFs while the WGC KEDF remained accurate. In Figure 10, we first plot G vs. d curves for the hcp Mg vacancy structure. In the benchmark KSDFT data, the original single-valued curve (in perfect hcp Mg) bifurcates into two branches, and the width of each branch is slightly wider than in the hcp Mg case. Notice that the upper branch corresponds to the original curve in hcp Mg and contains the majority of the data. The lower branch thus corresponds to the local vacancy region. The results for both fcc Al and bcc Li vacancy structures (not

shown) are very similar to the results for hcp Mg. We test Al_3Mg and again find a similar two-branch feature (Figure 11): G vs. d curve bifurcates, with neither of the two branches corresponding to the ones in pure fcc Al and hcp Mg, respectively. The bifurcation phenomenon explains the failure of vWGTF models, which have a one-to-one mapping between d and G. By contrast, the WGC KEDF successfully reproduces the bifurcation feature in all cases, which we find rather amazing and inspiring. Based on its well-known outstanding performance for simple metals, one may have conjectured its accurate KED as well. However, after many tests and applications of the WGC KEDF, studies of the KED on a pointwise level were lacking. The results here confirm that the WGC KEDF is accurate both on a pointwise level and an integrated level. This also highlights the importance of studying local quantities rather than just total kinetic energies.

We next explore other systems for which the WGC KEDF is insufficient, such as CD Si. In Figure 12, similar curves are plotted for CD Si. We again observe two main branches in the G vs. d distribution in KSDFT and the WGC KEDF surprisingly preserves this feature. However, we notice a bit larger discrepancy of absolute G values in this system. This may be one of the reasons why the WGC KEDF is not accurate for Si, when compared to KSDFT. Furthermore, the similar bifurcation structure in Si also indicates that the pointwise approach may be general and promising for materials other than simple metals, such as CD Si here. Analyzing and reproducing the bifurcation feature should be a key to make new KEDFs more accurate and transferable.

Finally, we expect isolated systems to possess a completely different character from extended systems. As an example, we examine the singlet state of the P_2 molecule. Since the WGC KEDF cannot converge in this case, only KSDFT data are presented. Moreover, the average density in the definition of d is not well-defined. Here, we use ρ_{max} instead of ρ_0; this will not change any key properties since both are just constants. In Figure 13, we observe that the G values are more scattered and it is hard to sort out any structures or patterns. We also tried plotting G vs. other density variables, but found no further insight.

E. Discussion and future work

In this section, we discuss possible improvements, which we hope this current work will inspire. In the previous section, we displayed the bifurcation feature in G vs. d distributions in various systems. We concluded that it is impossible to use only d to predict G in such situations. Our simple vWGTF models fail because they are all based on a one-to-one mapping between G and d. We questioned GGA KEDFs in an earlier section for a similar failure, but for the independent variable s instead of d. We have over-simplified when approximating G, which ought to be a functional of the electron density. Even when simplifying G to a function, more density variables (such as s and l) should be included in G. We find that G vs. l distributions feature relatively well-defined distributions (by contrast, G vs. s distributions generally have more complicated structures; see Figure 6 for example). For instance, the bifurcation occurs in l vs. d (Figure 14) and in G vs. l (Figure 15) distributions for CD Si and the Mg

vacancy structure, respectively. Moreover, we found that branches correspond perfectly: data points in the upper branch of G vs. d plot also lie in the upper branch of the l vs. d plot. This strongly suggests using both d and l to predict G. One way to do this is to combine d and l to form a new density variable, which can uniquely determine corresponding G values, *i.e.*, two branches can be unified if plotting G against this new density variable. Unfortunately, after several attempts, we were still unable to find such a variable, even after trying to include s, as well.

Another way is to define a multivariate function, such as $G(d,l)$. For this, we try to average two branches of $G(d)$ with the weights depending on l. More specifically, we design $G = G(d,l) = G_u(d) \cdot W_u + G_l(d) \cdot W_l$, where $G_u(d)$ and $G_l(d)$ are determined by the upper and lower branches, respectively. W_u and W_l take the form as $W_u = w_u / (w_u + w_l)$ and $W_l = w_l / (w_u + w_l)$, where w_u and w_l are rapidly decaying functions such as $w_u = e^{-(l - L_u(d))^2}$ and $w_l = e^{-(l - L_l(d))^2}$, with $L_u(d)$ and $L_l(d)$ defined similarly as $G_u(d)$ and $G_l(d)$, respectively. Using this function, G is determined with the correct function of d by making use of the local l value. We tested this model on CD Si, metal vacancies, and the Al_3Mg alloy, and found that non-self-consistent kinetic energy errors are greatly reduced to within 0.5%. However, the $G(d)$ and $L(d)$ branch functions are not transferable for different systems. Furthermore, we again encountered convergence issues when carrying out self-consistent calculations with this multivariate G function. Adding s or l into KEDFs generally leads to numerical difficulties in self-consistent optimizations, which makes developing accurate single-point KEDFs more difficult.

This work is also closely related to the recently proposed density decomposition method.[29] On one hand, the quality of the density decomposition depends on the scale function, which aims to distinguish and separate localized and delocalized electron densities. An accurate pointwise-based KEDF and its corresponding OF-ELF (Equation (8)) may help to construct a better scale function. On the other hand, accurate single-point KEDFs are needed for the localized KEDF and the KEDF interaction terms (see ref. 29 for details). We are now testing different GGA KEDFs, as well as our new vWGTF models, for these terms as a means of further improving the density decomposition method for KEDF development.

V. Conclusions

Previous KEDF assessments of quality have mostly focused on the integrated total (kinetic) energy or resultant physical properties. Here, we argued that accurate pointwise quantities are important and useful criteria for constructing KEDFs. We first proposed a new KEDF development scheme based on a pointwise KED analysis. We investigated the relationship between G and the reduced density d, reduced gradient s, and reduced Laplacian l in KSDFT. For various simple metals, in particular bulk Al, Mg, and Li, we found a strong correspondence between G and d; data points from different phases formed a well-defined single-valued function. In contrast, G vs. s was usually multi-valued, which calls into question the validity of using s as the sole variable when constructing enhancement factors. Through fitting a small set of data for G vs. d or ELF vs. d, the resulting models significantly improved

non-self-consistent kinetic energies with MAEs within 1%. The WGC KEDF produced the best results (<0.1%), while previously proposed GGA KEDFs generally led to errors of about 3-6%.

We also performed a thorough test of self-consistent optimizations with our models and various GGA KEDFs. Unfortunately, most GGA KEDFs had serious convergence problems. The optimized densities showed unphysical distributions: extremely small densities around the nuclei, as well as sharp density changes. The numerical evaluation of gradients or Laplacians using FFTs was no longer reasonable for these unphysical densities. Consequently, we believe that the self-consistent results obtained could not be considered as the real physical outcomes of these GGA KEDFs. We therefore concluded that self-consistent optimizations are rather cumbersome when density gradients are involved. In contrast, our new vWGTF models converged readily and gave reasonable self-consistent results for all perfect bulk systems. Errors for equilibrium volumes and bulk moduli were within 5%, and phase ordering energies also agreed well with KSDFT benchmarks.

However, the vWGTF models showed unfortunate failures when calculating defective or alloyed systems. Plotting KSDFT G vs. d distributions in these samples showed a clear two-branch bifurcation feature. This feature therefore demonstrated the inadequacy of the current vWGTF models which approximated G as a simple function of d. The WGC KEDF, however, accurately reproduced the bifurcation feature, which also explained its accurate total energies and bulk properties for these

types of materials. We thus expect a single-point KEDF that can predict this bifurcation feature will provide more accurate kinetic energies and material properties than the current vWGTF models. We hope this study inspires more ideas for developing new KEDFs and thus further advance OFDFT, both theoretically and practically.

Acknowledgements

We thank the Office of Naval Research for supporting this research. We thank the Tigress High Performance Computing Center and Department of Defense HPCMP Open Research Systems for computing time. We also thank Dr. Youqi Ke and Dr. Valentin Karasiev for helpful discussions and Ms. Nari Baughman for critical reading of the manuscript. We also want to acknowledge early attempts reported in Vincent Ligneres's thesis[48] at checking pointwise data from KSDFT to gain insights into KEDF development.

References

1. W. Kohn and L. J. Sham, Phys. Rev. **140**, A1133 (1965).

2. P. Hohenberg and W. Kohn, Phys. Rev. **136**, B864 (1964).

3. Y. A. Wang and E. A. Carter, in *Theoretical Methods in Condensed Phase Chemistry*, edited by S. D. Schwartz (Kluwer, Dordrecht, 2000), p. 117.

4. L. Hung, E. A. Carter, Chem. Phys. Lett. **475**, 163 (2009).

5. E. Chacón, J. E. Alvarellos, and P. Tarazona, Phys. Rev. B **32**, 7868 (1985).

6. P. García-González, J. E. Alvarellos, and E. Chacón, Phys. Rev. B **53**, 9509 (1996).

7. P. García-González, J. E. Alvarellos, and E. Chacón, Phys. Rev. B **57**, 4857 (1998).

8. L. W. Wang and M. P. Teter, Phys. Rev. B **45**, 13196 (1992).

9. Y. A. Wang, N. Govind, and E. A. Carter, Phys. Rev. B **58**, 13465 (1998); **64**, 129901-1(E) (2001).

10. Y. A. Wang, N. Govind, and E. A. Carter, Phys. Rev. B **60**, 16350 (1999); **64**, 089903(E) (2001).

11. N. W. Ashcroft and N. D. Mermin, *Solid State Physics* (Holt Rinehart & Winston, Philadelphia, 1976).

12. W. A. Harrison, *Solid State Theory* (Dover, New York, 1980).

13. I. Shin, A. Ramasubramaniam, C. Huang, L. Hung, and E. A. Carter, Philos. Mag. 89, 3195 (2009).

14. I. Shin and E. A. Carter, Int. J. Plasticity **60**, 58 (2014).

15. I. Shin and E. A. Carter, Acta Materialia **64**, 198 (2014).

16. I. Shin and E. A. Carter, Phys. Rev. B **88**, 064106 (2013).

17. I. Shin and E. A. Carter, Modell. Simul. Mater. Sci. Eng. **20**, 015006 (2012).

18. L. Hung and E. A. Carter, Modell. Simul. Mater. Sci. Eng. **19**, 045002 (2011).

19. Q. Peng, X. Zhang, L. Hung, E. A. Carter, and G. Lu, Phys. Rev. B **78**, 054118 (2008).

20. R. L. Hayes, G. S. Ho, M. Ortiz, and E. A. Carter, Phil. Mag. **86**, 2343 (2006).

21. G. Ho and E. A. Carter, J. Comput. Theor. Nanos. **6**, 1236 (2009).

22. L. Hung and E. A. Carter, J. Phys. Chem. C **115**, 6269 (2011).

23. R. L. Hayes, M. Fago, M. Ortiz, and E. A. Carter, Multiscale Modeling and Simulation **4,** 359(2005).

24. N. Choly, G. Lu, W. E, and E. Kaxiras, Phy. Rev. B **71**, 094101 (2005).

25. S. C. Watson and P. A. Madden, PhysChemComm **1**, 1 (1998).

26. M. Chen, L. Hung, C. Huang, J. Xia, and E. A. Carter, Molecular Physics **111**, 3448 (2013).

27. C. Huang and E. A. Carter, Phys. Rev. B **81**, 045206 (2010).

28. J. Xia, C. Huang, I. Shin, and E. A. Carter, J. Chem. Phys. **136**, 084102 (2012).

29. J. Xia and E. A. Carter, Phys. Rev. B **86**, 235109 (2012).

30. I. Shin and E. A. Carter, J. Chem. Phys., **140**, 18A531 (2014).

31. J. Xia and E. A. Carter, Journal of Power Sources **254**, 62 (2014).

32. C. Huang and E. A. Carter, Phys. Rev. B **85**, 045126 (2012).

33. Y. Ke, F. Libisch, J. Xia, L.-W. Wang, and E. A. Carter, Phys. Rev. Lett. **111**, 066402 (2013).

34. Y. Ke, F. Libisch, J. Xia, and E. A. Carter, Phys. Rev. B **89**, 155112 (2014).

35. L. H. Thomas, Proc. Cambridge Philos. Soc. **23**, 542 (1927).

36. E. Fermi, Rend. Accad. Naz. Lincei **6**, 602 (1927).

37. E. Fermi, Z. Phys. **48**, 73 (1928).

38. C. F. von Weizsäcker, Z. Phys. **96**, 431 (1935).

39. D. Garcia-Aldea and J. E. Alvarellos, J. Chem. Phys. **127**, 144109 (2007).

40. V. V. Karasiev, R. S. Jones, S. B. Trickey, and F. E. Harris, in *New Developments in Quantum Chemistry*, edited by J. L. Paz and A. J. Herna'ndez (Research Signpost, Kerala, 2009), p. 25.

41. A. W. Götz, S. M. Beyhan, and L. Visscher, J. Chem. Theory Comput. **5**, 3161 (2009).

42. V. V. Karasiev, T. Sjostrom, and S. B. Trickey, Phys. Rev. B **86**, 115101 (2012).

43. V. V. Karasiev, D. Chakraborty, O. A. Shukruto, and S. B. Trickey, Phys. Rev. B **88**, 161108(R) (2013).

44. V. V. Karasiev and S. B. Trickey, Comput. Phys. Commun. **183**, 2519 (2012).

45. D. García-Aldea and J. E. Alvarellos, Phys. Chem. Chem. Phys. **14**, 1756 (2012).

46. T. Martín-Blas, D. García-Aldea and J. E. Alvarellos, J. Chem. Phys. **131**, 164117 (2009).

47. W. Yang, R. G. Parr, C. Lee, Phys. Rev. A **34**, 4586 (1986).

48. V. Ligneres, Ph.D. thesis, Princeton University, 2008.

49. B. Silvi and A. Savin, Nature (London) **371**, 683 (1994).

50. A. D. Becke and K. E. Edgecombe, J. Chem. Phys. **92**, 5397 (1990).

51. J. Sun, B. Xiao, Y. Fang, R. Haunschild, P. Hao, A. Ruzsinszky, G. I. Csonka, G. E. Scuseria, and J. P. Perdew, Phys. Rev. Lett. **111**, 106401 (2013).

52. V. V. Karasiev, R. S. Jones, S. B. Trickey, and F. E. Harris, Phys. Rev. B **80**, 245120 (2009).

53. P. de Silva, J. Korchowiec, N. J. S. Ram, and T. A. Wesolowski, CHIMIA, **67**, 253 (2013).

54. R. M. Dreizler, E. K. U. Gross, *Density functional theory: an approach to the quantum many-Body problem*, Springer, Berlin (1990).

55. R. F. W. Bader and H. Essén, J. Chem. Phys. **80**, 1943 (1984).

56. X. Gonze, J.-M. Beuken, R. Caracas, F. Detraux, M. Fuchs, G.-M. Rignanese, L. Sindic, M. Verstraete, G. Zerah, F. Jollet, M. Torrent, A. Roy, M. Mikami, Ph. Ghosez, J.-Y. Raty, D. C. Allan, Comput. Mater. Sci. **25**, 478 (2002).

57. G. Ho, V. L. Ligneres, and E. A. Carter, Comput. Phys. Commun. **179**, 839 (2008).

58. L. Hung, C. Huang, I. Shin, G. Ho, V. L. Ligneres, E. A. Carter, Comput. Phys. Comm. **181**, 2208 (2010).

59. M. Chen *et al.* in preparation.

60. J. P. Perdew, K. Burke, M. Ernzerhof, Phys. Rev. Lett. **77**, 3865 (1996).

61. B. Zhou, Y. A. Wang, E. A. Carter, Phys. Rev. B **69**, 125109 (2004).

62. C. Huang, E. A. Carter, Phys. Chem. Chem. Phys. **10**, 7109 (2008).

63. H. J. Monkhorst and J. D. Pack, Phys. Rev. B **13**, 5188 (1976).

64. G. K. Chan, A. J. Cohen, and N. C. Handy, J. Chem. Phys. **114**, 631 (2001).

65. A. Berk, Phys. Rev. A **28**, 1908 (1983).

66. N. Govind, J. Wang, and H. Guo, Phys. Rev. B **50**, 11175 (1994).

67. K. Yonei, J. Phys. Soc. Jpn. **22**, 1127 (1967).

68. Y. Tomishima and K. Yonei, J. Phys. Soc. Jpn. **21**, 142 (1966).

69. D. A. Kirzhnits, Sov. Phys. JETP **5**, 64 (1957).

70. H. Lee, C. Lee, and R. G. Parr, Phys. Rev. A **44**, 768 (1991).

71. A. E. Depristo and J. D. Kress, Phys. Rev. A **35**, 438 (1987).

72. A. E. Depristo and J. D. Kress, J. Chem. Phys. **86**, 1425 (1987).

73. H. Ou-Yang and M. Levy, Int. J. Quantum Chem. **40**, 379 (1991).

74. J. P. Perdew and Y. Wang, Phys. Rev. B **33**, 8800 (1986).

75. D. J. Lacks and R. G. Gordon, J. Chem. Phys. **100** 4446 (1994).

76. J. P. Perdew, J. A. Cevary, S. H. Vosko, K. A. Jackson, M. R. Pederson, D. J. Singh, and C. S. H. Fiolhais, Phys. Rev. B **46**, 6671 (1992).

77. A. Lembarki and H. Chermette, Phys. Rev. A **50**, 5328 (1994).

78. F. Tran and T. A. Wesolowski, Int. J. Quantum Chem. **89**, 441 (2002)

79. V. V. Karasiev, S. B. Trickey, and F. E. Harris, J. Comput.-Aided Mater. Des. **13**, 111 (2006).

80. M. Ernzerhof, J. Mol. Struct.: THEOCHEM **501**, 59 (2000).

81. J. P. Perdew, Phys. Lett. A **165**, 79 (1992).

82. A. D. Becke, J. Chem. Phys. **85**, 7184 (1986).

83. A. D. Becke, J. Chem. Phys. **85**, 4524 (1986).

84. A. J. Thakkar, Phys. Rev. A **46**, 6920 (1992).

85. B. Zhou, V. Ligneres, and E. A. Carter, J. Chem. Phys. **122**, 044103 (2005).

86. F. D. Murnaghan, Proc, Natl, Acad. Sci. USA **30**, 244 (1944).

87. M. J. Gillan, J. Phys.: Condens. Matter 1, 689 (1989).

Tables

Table I. KEDF non-self-consistent total kinetic energy errors and MAEs (in %) with respect to KSDFT benchmarks for bulk Al, Mg, and Li in the fcc, bcc, hcp, and sc structures at KSDFT equilibrium volumes.

KEDF	fcc Al	hcp Al	bcc Al	sc Al	hcp Mg	fcc Mg	bcc Mg	sc Mg	bcc Li	fcc Li	hcp Li	sc Li	MAE
vW	-91.75	-91.96	-92.02	-85.52	-90.30	-90.57	-90.87	-88.08	-93.39	-93.34	-93.34	-93.47	91.22
Thak	-5.77	-5.92	-6.18	-7.19	-6.14	-6.26	-6.04	-8.28	-5.16	-5.22	-5.23	-5.15	6.05
TF	-5.24	-5.35	-5.57	-7.47	-5.89	-6.05	-5.89	-8.13	-4.79	-4.84	-4.85	-4.80	5.74
DK	-4.44	-4.57	-4.79	-5.92	-5.04	-5.22	-5.10	-6.98	-4.12	-4.16	-4.17	-4.14	4.89
PW86	-4.39	-4.53	-4.76	-5.98	-4.87	-5.06	-4.91	-6.96	-4.13	-4.18	-4.18	-4.15	4.84
TF1/9vW	-4.32	-4.46	-4.69	-5.86	-4.81	-5.00	-4.87	-6.81	-4.05	-4.10	-4.10	-4.07	4.76
P92	-4.32	-4.46	-4.68	-5.86	-4.81	-5.00	-4.87	-6.80	-4.05	-4.10	-4.10	-4.07	4.76
TW02	-4.27	-4.40	-4.63	-5.66	-4.83	-5.02	-4.90	-6.72	-4.02	-4.06	-4.07	-4.05	4.72
PW91	-4.25	-4.39	-4.62	-5.55	-4.84	-5.02	-4.91	-6.66	-3.99	-4.04	-4.04	-4.02	4.69
B86B	-4.24	-4.37	-4.60	-5.59	-4.80	-4.99	-4.87	-6.67	-3.99	-4.04	-4.04	-4.02	4.69
LC94	-4.24	-4.38	-4.60	-5.58	-4.80	-4.99	-4.87	-6.66	-3.99	-4.03	-4.04	-4.02	4.68
LLP	-4.23	-4.37	-4.59	-5.57	-4.81	-5.00	-4.89	-6.66	-3.98	-4.03	-4.03	-4.01	4.68
B86A	-4.23	-4.37	-4.59	-5.60	-4.78	-4.97	-4.85	-6.67	-3.99	-4.04	-4.04	-4.02	4.68
E00	-4.20	-4.34	-4.57	-5.72	-4.59	-4.78	-4.65	-6.63	-3.92	-3.97	-3.97	-3.94	4.61
OL1	-4.12	-4.25	-4.47	-5.52	-4.62	-4.82	-4.71	-6.52	-3.89	-3.94	-3.95	-3.92	4.56

DK87	-4.12	-4.26	-4.50	-5.32	-4.62	-4.81	-4.69	-6.51	-3.88	-3.92	-3.93	-3.90	4.54
OL2	-3.72	-3.85	-4.06	-5.15	-4.27	-4.49	-4.40	-6.13	-3.58	-3.63	-3.63	-3.62	4.21
TF1/5vW	-3.59	-3.74	-3.98	-4.58	-3.95	-4.16	-4.06	-5.75	-3.46	-3.51	-3.51	-3.49	3.98
PBE2	3.20	2.88	2.63	8.31	3.30	2.88	2.67	4.13	1.89	1.89	1.88	1.73	3.12
TFvW	3.01	2.69	2.41	7.01	3.82	3.38	3.25	3.79	1.83	1.83	1.82	1.73	3.05
vWGTF1	-0.05	-0.25	-0.30	0.68	0.42	0.18	0.11	0.09	-0.52	-0.53	-0.54	-0.52	0.35
vWGTF2	0.35	0.19	0.21	0.24	0.66	0.46	0.41	0.32	0.11	0.10	0.09	0.14	0.27
WGC	0.01	-0.02	-0.02	-0.03	0.20	0.10	0.07	-0.03	-0.07	-0.08	-0.06	-0.05	0.06

Table II. KEDF non-self-consistent total kinetic energy errors and MAEs (in %) with respect to KSDFT benchmarks for fcc Al, hcp Mg, and bcc Li vacancy structures, as well as Al_3Mg, at KSDFT geometries.

KEDF	Al_3Mg	Al Vac	Mg Vac	Li Vac	MAE
vW	-89.46	-91.09	-89.58	-92.49	90.66
Thak	-6.07	-5.70	-6.19	-5.52	5.87
TF	-5.74	-5.28	-6.02	-5.04	5.52
DK	-4.69	-4.40	-5.09	-4.27	4.61
PW86	-4.69	-4.35	-4.93	-4.31	4.57
TF1/9vW	-4.57	-4.29	-4.87	-4.21	4.49
P92	-4.57	-4.29	-4.86	-4.21	4.48
TW02	-4.47	-4.22	-4.87	-4.15	4.43
PW91	-4.42	-4.20	-4.87	-4.12	4.40
B86B	-4.43	-4.19	-4.84	-4.12	4.40
LC94	-4.42	-4.19	-4.85	-4.10	4.39
LLP	-4.42	-4.19	-4.84	-4.11	4.39
B86A	-4.43	-4.18	-4.82	-4.12	4.39
E00	-4.42	-4.16	-4.64	-4.08	4.33
OL1	-4.30	-4.07	-4.67	-4.01	4.26
DK87	-4.29	-4.05	-4.64	-4.01	4.25
OL2	-3.90	-3.68	-4.31	-3.65	3.89
TF1/5vW	-3.63	-3.50	-3.94	-3.54	3.65
PBE2	5.25	3.88	3.97	2.69	3.95
TFvW	4.80	3.63	4.40	2.47	3.83

vWGTF1	-0.61	-0.63	0.06	-0.96	0.57
vWGTF2	-0.87	-0.65	-0.01	-0.62	0.54
WGC	0.05	0.03	0.22	-0.09	0.10

Table III. Equilibrium volumes (V_0), bulk moduli (B), and equilibrium total energies ($E_{\min}$) for various Al phases calculated by self-consistent KSDFT and OFDFT. Only OFDFT results for numerically stable KEDFs are reported (see Sec. IV B for details); same for Tables IV and V.

		fcc	hcp	bcc	sc
V_0 (Å^3)	KSDFT	16.575	16.733	17.025	19.937
	WGC	16.590	16.657	16.839	20.368
	vWGTF1	16.859	16.859	16.882	20.715
	vWGTF2	16.872	16.871	16.876	23.486
	TFvW	17.452	17.418	17.464	19.258
	TF1/5vW	19.024	18.884	19.234	22.112
	TF1/9vW	21.951	22.420	22.311	26.569
	E00	21.291	21.511	21.553	24.935
	P92	21.928	22.377	22.283	26.144
B (GPa)	KSDFT	77	75	70	57
	WGC	75	73	70	57
	vWGTF1	85	84	83	50
	vWGTF2	76	76	75	26
	TFvW	106	115	106	88
	TF1/5vW	46	44	44	32
	TF1/9vW	23	16	23	13
	E00	29	24	29	20
	P92	23	17	23	15
$E_{\min}$ (eV/atom)	KSDFT	-57.202	0.024	0.081	0.334

	WGC	-57.188	0.016	0.074	0.324
	vWGTF1	-57.231	-0.004	0.042	0.472
	vWGTF2	-57.119	-0.006	0.053	0.232
	TFvW	-56.716	-0.004	0.021	0.799
	TF1/5vW	-59.036	0.001	0.015	0.250
	TF1/9vW	-59.983	0.000	0.003	0.106
	E00	-59.487	0.000	0.006	0.133
	P92	-59.979	-0.002	0.003	0.107

Table IV. Equilibrium volumes (V_0), bulk moduli (B), and equilibrium total energies (E_{min}) for various Mg phases calculated by self-consistent KSDFT and OFDFT.

		hcp	fcc	bcc	sc
V_0 (Å^3)	KSDFT	22.899	23.073	22.839	27.107
	WGC	23.083	23.082	22.967	27.278
	vWGTF1	23.875	23.877	23.773	26.819
	vWGTF2	23.570	23.472	23.469	26.896
	TFvW	25.172	25.221	25.121	27.189
	TF1/5vW	23.870	23.874	23.656	27.017
	TF1/9vW	24.806	24.813	24.465	29.113
	E00	24.955	24.958	24.633	28.772
	P92	24.802	24.809	24.453	29.096
B (GPa)	KSDFT	38	38	38	24
	WGC	37	37	37	23
	vWGTF1	38	38	38	27
	vWGTF2	37	37	37	24
	TFvW	38	37	38	31
	TF1/5vW	28	28	28	18
	TF1/9vW	22	22	21	11
	E00	23	23	22	13
	P92	22	22	21	11
E_{min} (eV/atom)	KSDFT	-24.246	0.013	0.029	0.408
	WGC	-24.217	0.007	0.020	0.391
	vWGTF1	-24.221	0.001	0.011	0.396
	vWGTF2	-24.184	0.002	0.013	0.387
	TFvW	-24.006	-0.001	0.006	0.414
	TF1/5vW	-25.069	-0.001	0.010	0.249
	TF1/9vW	-25.473	-0.001	0.012	0.185

	E00	-25.187	-0.001	0.011	0.193
	P92	-25.471	-0.001	0.012	0.185

Table V. Equilibrium volumes (V_0), bulk moduli (B), and equilibrium total energies (E_{min}) for various Li phases calculated by self-consistent KSDFT and OFDFT.

		bcc	fcc	hcp	sc
V_0 (Å^3)	KSDFT	19.397	19.308	19.324	19.932
	WGC	19.402	16.658	19.328	19.978
	vWGTF1	19.490	19.400	19.416	20.082
	vWGTF2	19.515	19.423	19.439	20.120
	TFvW	20.197	20.109	20.119	20.906
	TF1/5vW	17.644	17.460	17.488	18.684
	TF1/9vW	16.947	16.708	16.757	18.176
	E00	17.251	17.024	17.071	18.410
	P92	16.952	16.713	16.759	18.178
B (GPa)	KSDFT	16	17	17	17
	WGC	16	17	17	17
	vWGTF1	16	17	17	17
	vWGTF2	16	17	17	17
	TFvW	16	16	16	29
	TF1/5vW	18	18	18	18
	TF1/9vW	18	19	19	19
	E00	18	18	18	19
	P92	18	19	19	19
E_{min} (eV/atom)	KSDFT	-7.550	-0.001	0.000	0.136
	WGC	-7.543	-0.001	0.000	0.137
	vWGTF1	-7.559	-0.001	-0.001	0.136
	vWGTF2	-7.537	-0.001	-0.001	0.137
	TFvW	-7.499	0.000	0.000	0.132
	TF1/5vW	-7.748	-0.004	-0.004	0.125
	TF1/9vW	-7.836	-0.006	-0.005	0.117
	E00	-7.778	-0.005	-0.004	0.119
	P92	-7.836	-0.006	-0.005	0.117

Table VI. Vacancy formation energies (E_{vf}) for fcc Al, hcp Mg, and bcc Li calculated by self-consistent KSDFT and OFDFT with the WGC and vWGTF KEDFs.

E_{vf} (eV)	fcc Al	hcp Mg	bcc Li
KSDFT	0.722	0.945	1.028
OFDFT-WGC	0.808	0.983	1.019
OFDFT-vWGTF1	-4.886	-0.811	0.753
OFDFT-vWGTF2	-10.426	-2.539	0.509

Table VII. Equilibrium volume (V_0), bulk modulus (B), and alloy formation energy (E_{fm}) for Al_3Mg calculated by self-consistent KSDFT and OFDFT, with the WGC and vWGTF KEDFs.

	B (GPa)	V_0 (Å^3)	E_{fm} (eV/atom)
KSDFT	63	71.828	-0.019
OFDFT-WGC	64	71.812	-0.016
OFDFT-vWGTF1	67	74.292	-0.174
OFDFT-vWGTF2	57	75.078	-0.384

Figures

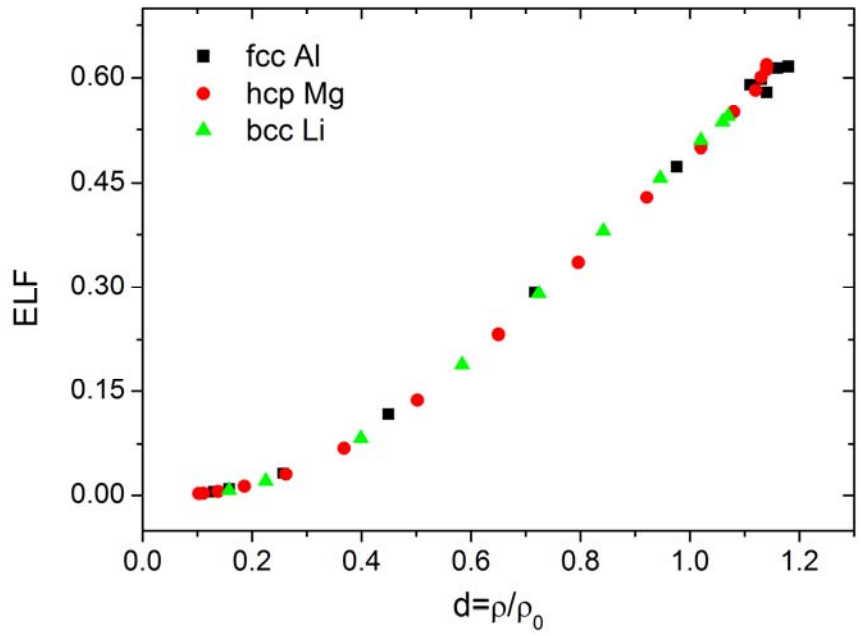

Figure 1. ELF vs. the reduced density (*d*) in fcc Al, hcp Mg, and bcc Li at equilibrium volumes calculated by KSDFT. Data points are taken only along the bond axis, *i.e.*, <110> for fcc Al, $<11\bar{2}0>$ for hcp Mg, and <111> for bcc Li.

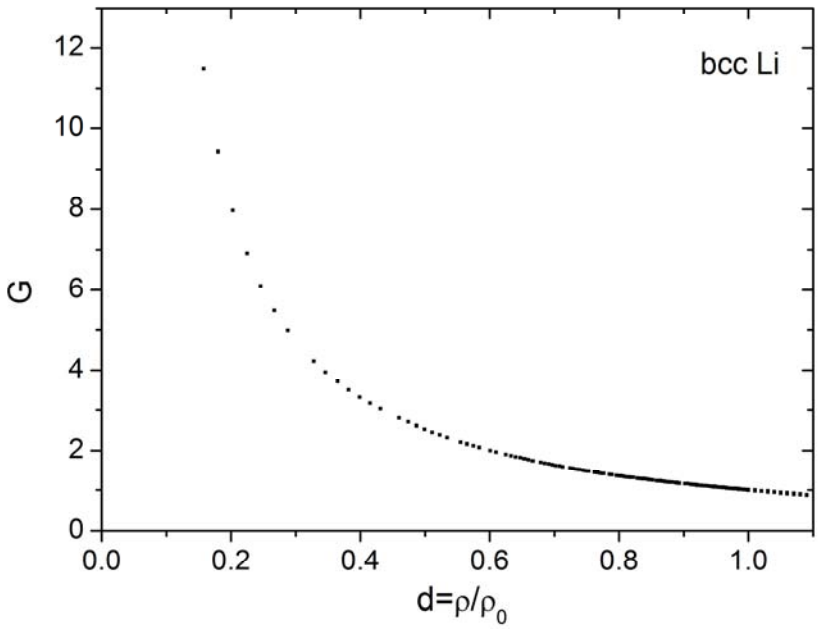

Figure 2. *G* vs. *d* in bcc Li at the equilibrium volume calculated by KSDFT. Data points are taken from all spatial points (on a numerical grid) in the unit cell.

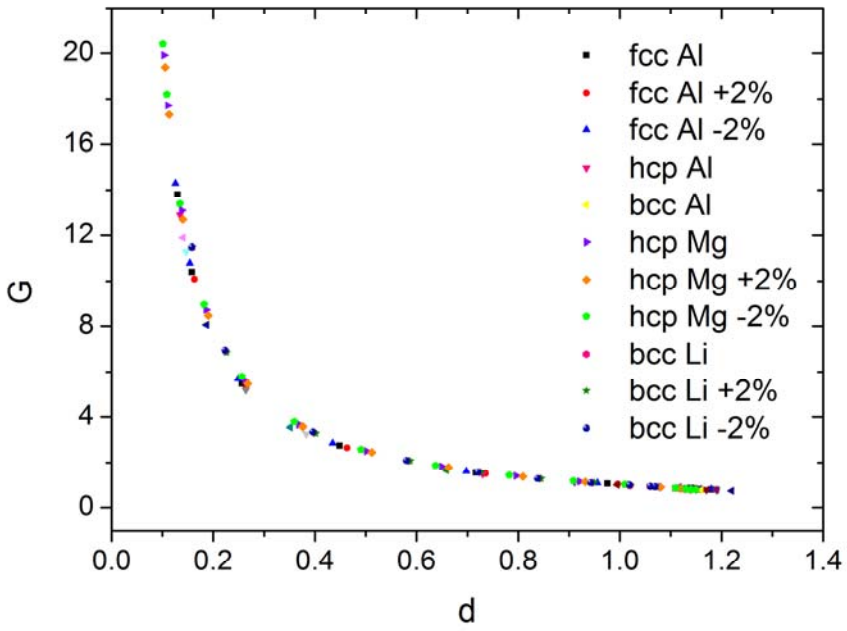

Figure 3. *G* vs. *d* in fcc Al, hcp Al, bcc Al, hcp Mg, and bcc Li at equilibrium volumes, as well as fcc Al, hcp Mg, and bcc Li at volumes changed $\pm 2\%$ around equilibrium volumes calculated by KSDFT. Data points are taken only along the bond axis, similar to Figure 1.

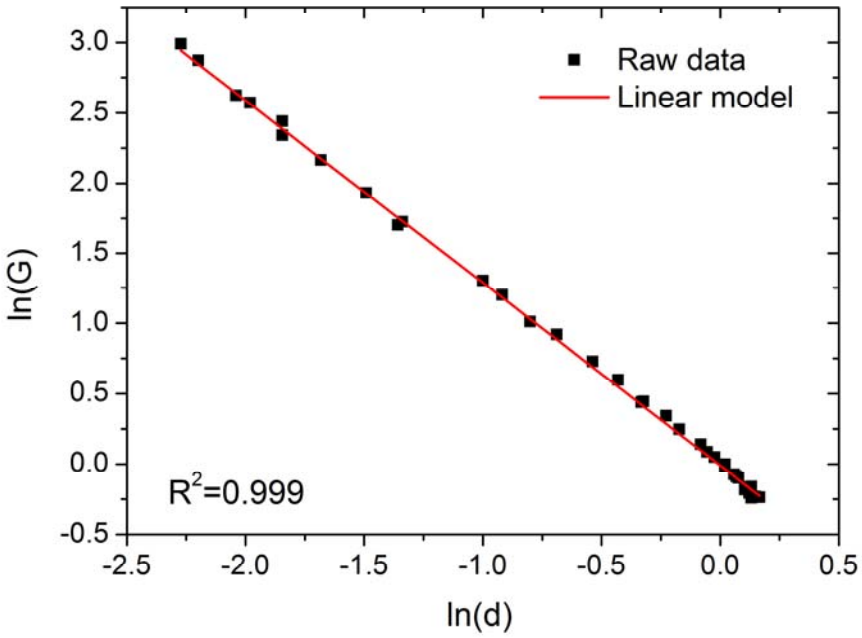

Figure 4. ln(*G*) vs. ln(*d*) in fcc Al, hcp Mg, and bcc Li at equilibrium volumes calculated by KSDFT and the linear model. Data points are taken only along the bond axis, similar to Figure 1.

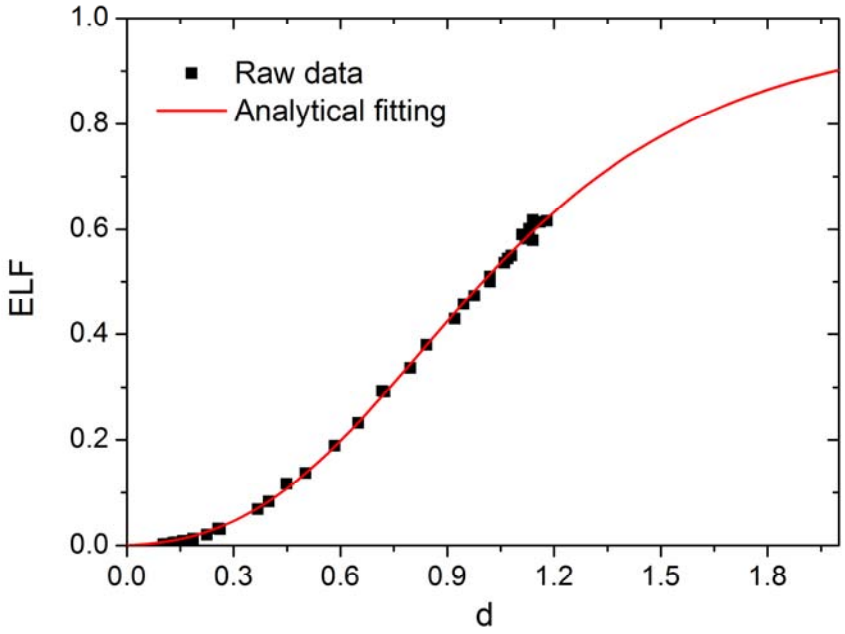

Figure 5. ELF vs. *d* for fcc Al, hcp Mg, and bcc Li at equilibrium volumes calculated by KSDFT, the analytical model (Equation 13), and the numerical interpolation model. Data points are taken only along the bond axis, similar to Figure 1.

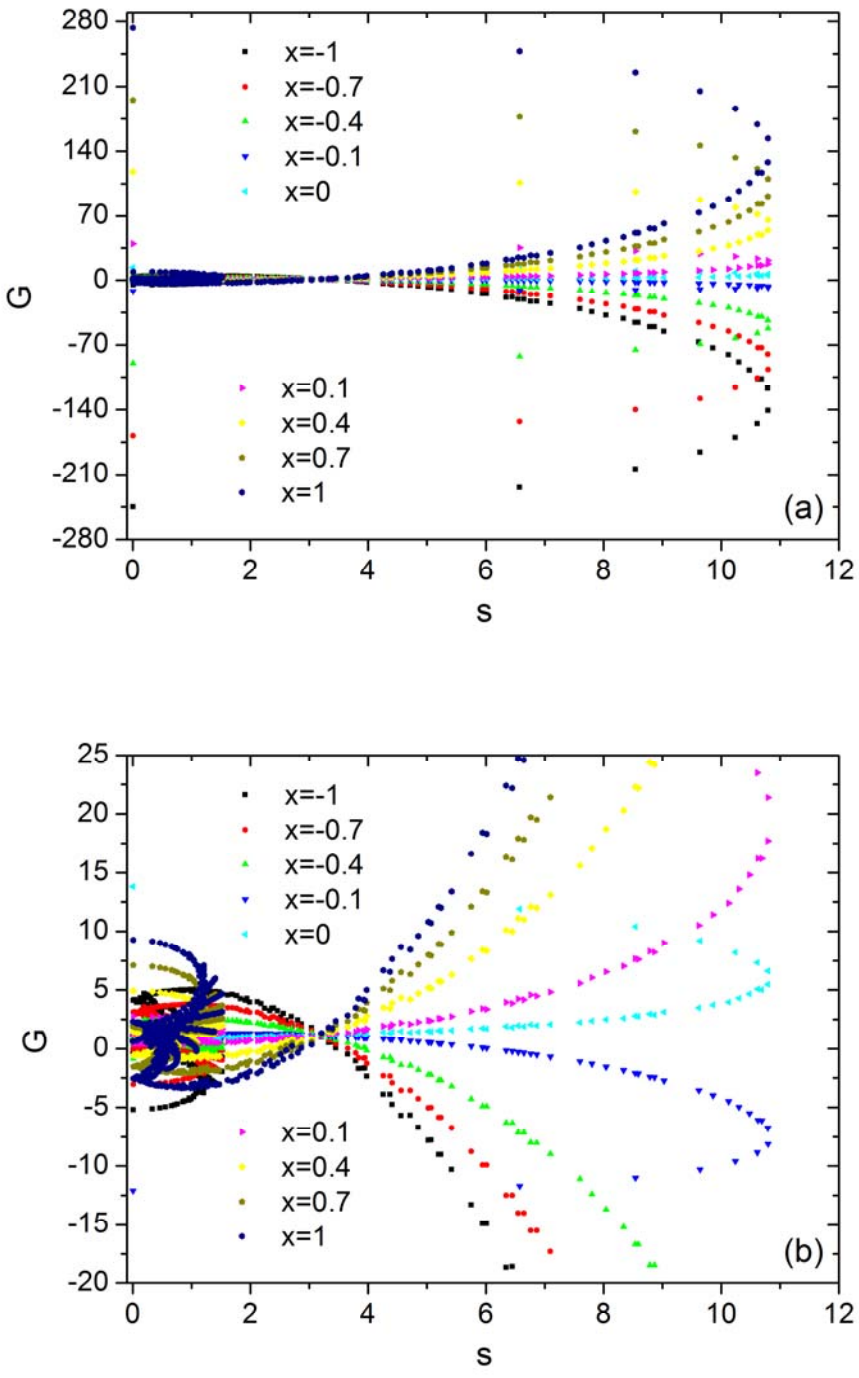

Figure 6. KSDFT G vs. s with τ calculated according to Equation (11) with multiple x values, (a) at a large scale and (b) at a fine scale. Data points are taken from all spatial points (on a numerical grid) in the unit cell of fcc Al at the KSDFT equilibrium volume.

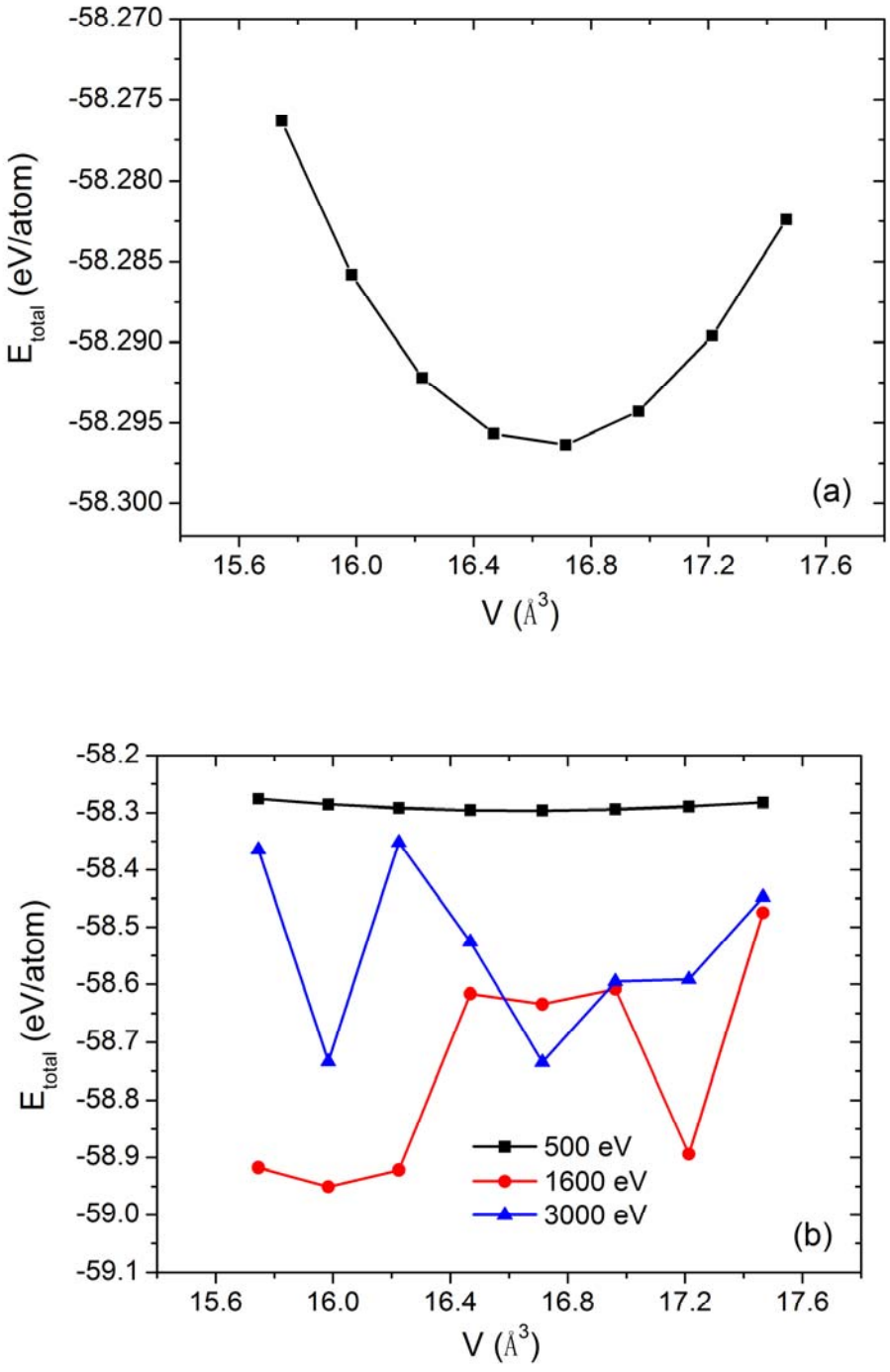

Figure 7. Total energies vs. volume per atom for fcc Al calculated by OFDFT with the PBE2 KEDF with (a) 500 eV kinetic energy cutoff and (b) 500, 1600, and 3000 eV kinetic energy cutoffs for the planewave basis.

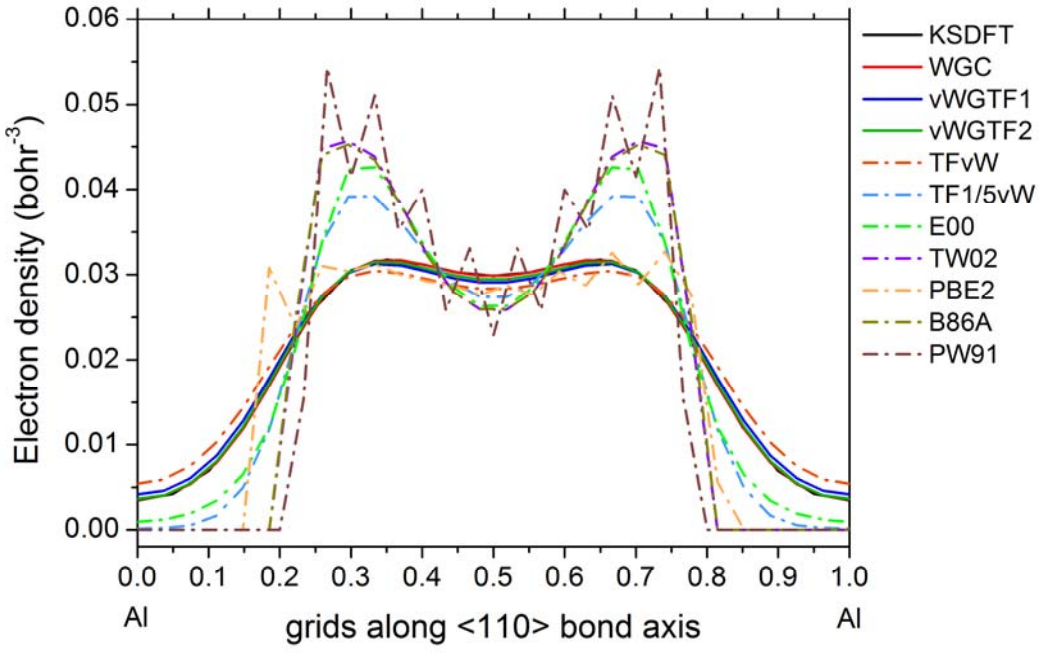

Figure 8. Self-consistent electron densities of fcc Al (at the KSDFT equilibrium volume) plotted along the <110> bond direction between two neighboring atoms (horizontal axis normalized to 1 and two Al atoms are at 0 and 1). KSDFT and OFDFT with the WGC and vWGTF models, as well as TFvW, TF1/5vW, E00, TW02, PBE2, B86A, and PW91 results are displayed. OFDFT calculations employ an increased energy cutoff (6000 eV) to achieve denser grids.

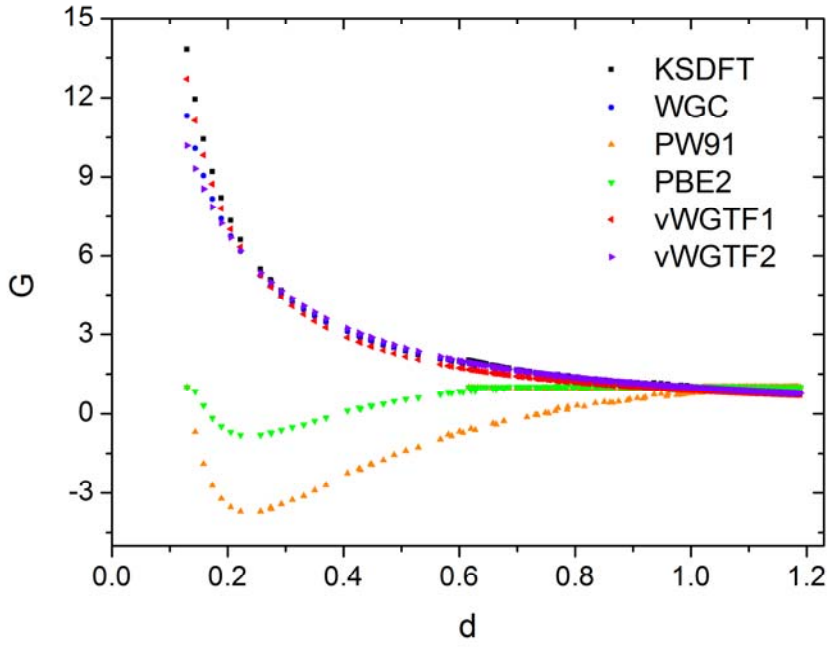

Figure 9. G (Equation (7)) vs. d (ρ/ρ_0) in fcc Al (at the KSDFT equilibrium volume) calculated by KSDFT and OFDFT with the WGC, vWGTF1, vWGTF2, PW91, and PBE2 KEDFs. The following conditions are applied in Figure 9 through Figure 12: OFDFT G values are non-self-consistently calculated using the self-consistently optimized KSDFT density; data points are taken from all spatial points (on a numerical grid) in the unit cell.

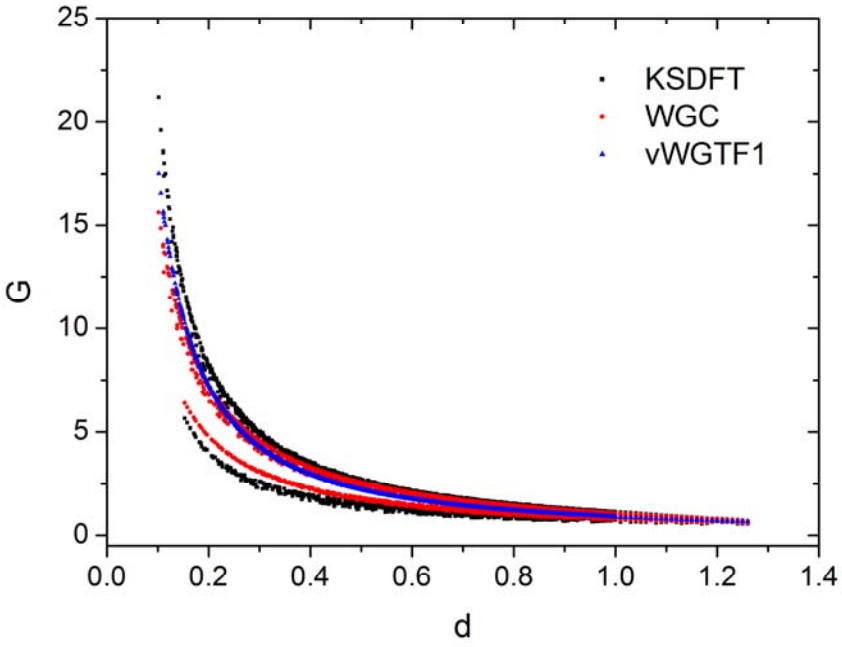

Figure 10. *G* vs. *d* in the Mg vacancy structure (at the KSDFT geometry) calculated by KSDFT and OFDFT with the WGC and vWGTF1 KEDFs.

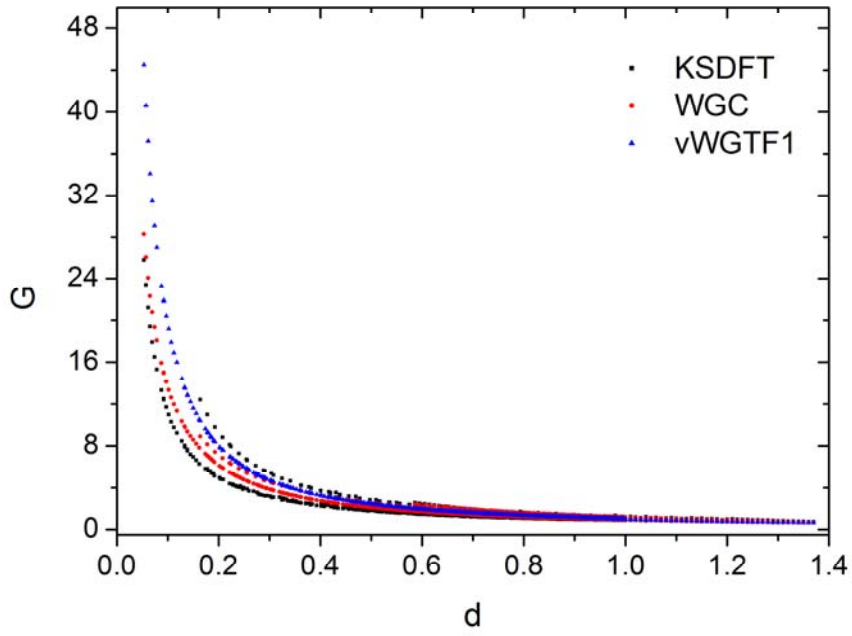

Figure 11. *G* vs. *d* in Al_3Mg (at the KSDFT equilibrium volume) calculated by KSDFT and OFDFT with the WGC and vWGTF1 KEDFs.

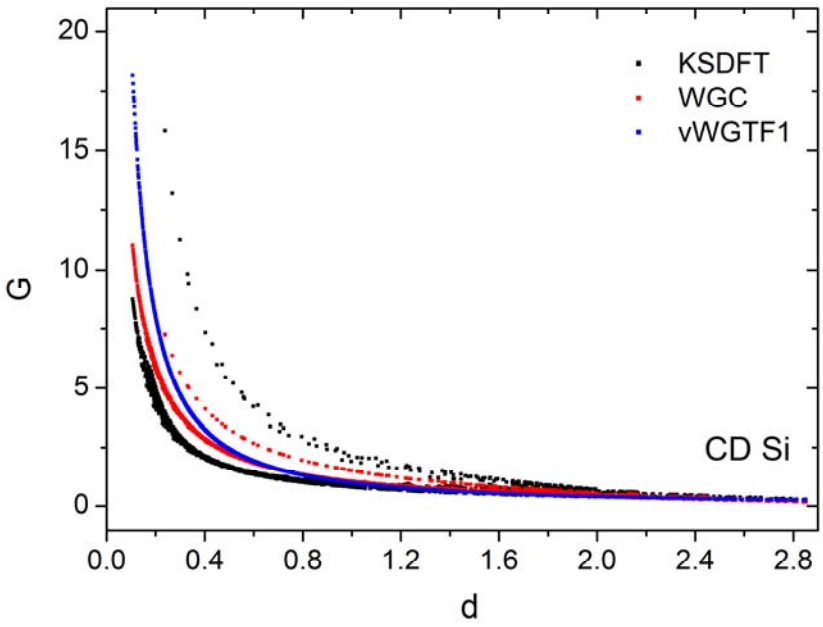

Figure 12. *G* vs. *d* in CD Si (at the KSDFT equilibrium volume) calculated by KSDFT and OFDFT with the WGC and vWGTF1 KEDFs.

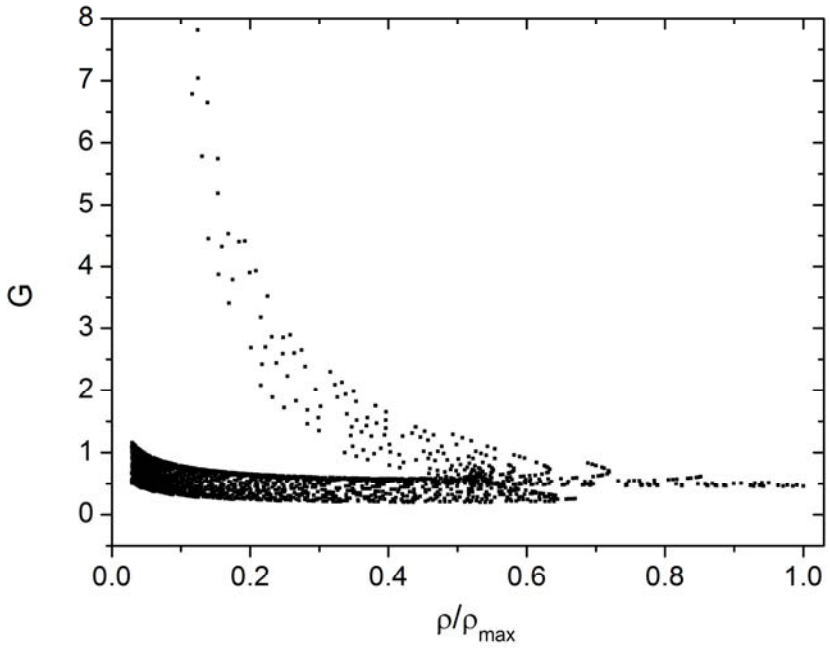

Figure 13. G vs. ρ/ρ_{max} in singlet P_2 at the KSDFT equilibrium bond length and using the density calculated by KSDFT. Data points are taken from all spatial points (on a numerical grid) where density is larger than 0.005 $bohr^{-3}$.

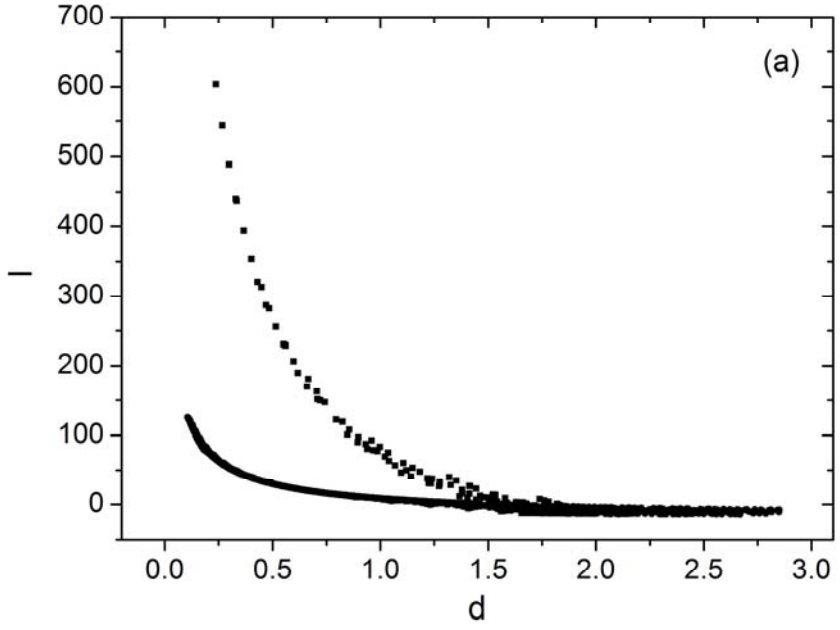
(a)
I
d
700
600
500
400
300
200
100
0
0.0
0.5
1.0
1.5
2.0
2.5
3.0

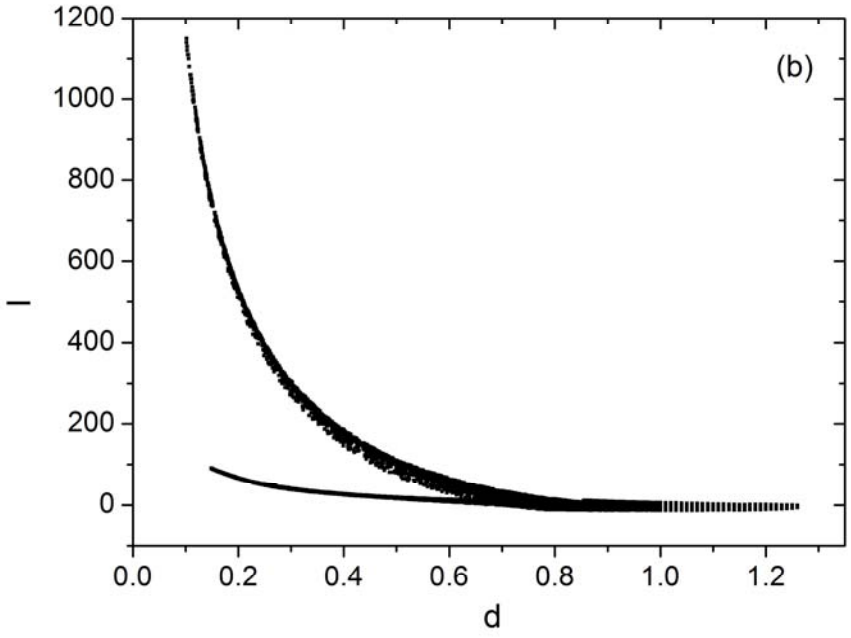
(b)
I
d
1200
1000
800
600
400
200
0
0.0
0.2
0.4
0.6
0.8
1.0
1.2

Figure 14. Reduced Laplacian *l* vs. *d* in (a) CD Si (at the equilibrium volume) and (b) Mg vacancy structure, calculated by KSDFT. Data points are taken from all spatial points (on a numerical grid) in the unit cell.

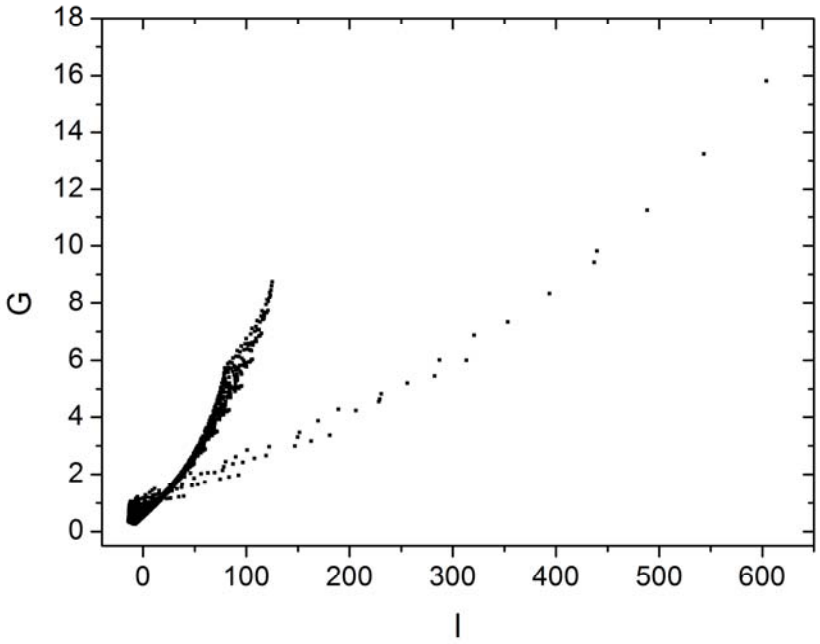

Figure 15. *G* vs. *l* in CD Si at the equilibrium volume calculated by KSDFT. Data points are taken from all spatial points (on a numerical grid) in the unit cell.